CERN-ACC-2019-0029

February 6, 2019

Detailed review of the LHC optics commissioning for the nonlinear era

E.H. Maclean[1,2], *R. Tomás*[2] *and F.S. Carlier*[2] *, M.S Camillocci*[2] *, J. Coello de Portugal*[2] *, E. Fol*[2] *, K. Fuchsberger*[2] *, A. Garcia-Tabares Valdivieso*[2] *, M. Giovannozzi*[2] *, M. Hofer*[2] *, L. Malina*[2] *, T.H.B. Persson*[2] *, P.K. Skowronski*[2] *, A. Wegscheider*[2]

[1] University of Malta, Msida, Malta

[2] CERN, Geneva, Switzerland

Abstract

In 2017, optics commissioning strategy for low-β^* operation of the CERN Large Hadron Collider (LHC) underwent a major revision. This was prompted by a need to extend the scope of beam-based commissioning at high-energy, beyond the exclusively linear realm considered previously, and into the nonlinear regime. It also stemmed from a recognition that, due to operation with crossing angles in the experimental insertions, the linear and nonlinear optics quality were intrinsically linked through potentially significant feed-down at these locations. Following the usual linear optics commissioning therefore, corrections for (normal and skew) sextupole and (normal and skew) octupole errors in the high-luminosity insertions were implemented. For the first time, the LHC now operates at top-energy with beam-based corrections for nonlinear dynamics, and for the effect of the crossing-scheme on beta-beating and dispersion. The new commissioning procedure has improved the control of various linear and nonlinear characteristics of the LHC, yielding clear operational benefits. This report gives a detailed account of the beam-based measurements carried out during the experimental campaigns.

Keywords

LHC, linear optics, nonlinear dynamics, insertion regions, optics commissioning

Contents

1 Introduction

Control of linear optics is a key operational concern at the CERN Large Hadron Collider (LHC). Machine protection, as well as an equitable distribution of delivered luminosity to the various High Energy Physics (HEP) apparatus, require tight constraints on optics quality. During the 2012-2016 period, development of new tools and methodology for LHC beam commissioning [1–4] allowed an unprecedented degree of control for hadron colliders to be achieved over linear optics [5–7]. In 2017 however, a major revision to the commissioning strategy for low-β^* optics was introduced. The objective of this change was to extend LHC optics commissioning into the nonlinear regime.

As β^* is reduced, the impact of magnetic errors in low-β^* insertions (IRs) increase substantially. Nonlinear errors in such insertions were a concern during design and construction of the Tevatron [8], RHIC [9] and LHC [10] high-luminosity insertions. Beam-based optimization of lifetime using nonlinear corrector magnets in the experimental IRs also yielded operational benefits at the RHIC collider [11, 12]. In the High-Luminosity LHC (HL-LHC) [13] compensation of nonlinear errors in experimental IRs is expected to be an operational necessity [14–16], with similar limitations expected for SuperKEKB [17]. Control of IR-nonlinearities is also a key ingredient in the design and development of the Future Circular Collider (FCC) lattice [18–20]. Prior to 2017 however, the LHC operated without any dedicated correction for nonlinear errors in its low-β^* experimental insertions.

In 2016 the LHC operated at $\beta^* = 0.4\,\mathrm{m}$ in the ATLAS (IR1) and CMS (IR5) insertions, and studies performed that year made it apparent that an operational impact from IR-nonlinearities should be expected. Of greatest operational relevance, direct measurements of amplitude detuning via AC-dipole excitation (following the method described in [21]) demonstrated that at $\beta^* = 0.4\,\mathrm{m}$ the tune-spread generated by normal octupole errors in LHC IRs was comparable to that purposefully introduced by Landau octupoles in the arcs to provide Landau damping [22]. Due to the β^* dependence of tune-spread generated in the IRs, this leads to a radical distortion of tune-footprint through the operational cycle. This is illustrated in Fig. 1, which shows a simplified picture of footprint evolution through a simulated β^* squeeze. It is seen that for $\beta^* \lesssim 0.4\,\mathrm{m}$ the footprint generated through the combination of Landau octupoles and IR-tunespread (red) differs substantially from the desired footprint (grey). Distortions in tune-footprint on the level observed are expected to influence the understanding and mitigation of instabilities [22]. Indeed during dedicated studies in 2016 a clear effect of the IR-octupoles was observed on the instability threshold at $0.4\,\mathrm{m}$ [23]. In 2017 the LHC initially operated at $\beta^* = 0.4\,\mathrm{m}$, then $0.3\,\mathrm{m}$. In 2018 it has operated down to $\beta^* = 0.25\,\mathrm{m}$. There is thus a strong motivation to compensate IR-octupole errors in the LHC.

Linear coupling can also cause substantial changes to detuning coefficients [21, 24–26], and plays a significant role in the generation of amplitude-dependent closest tune approach [24, 27–30]. Such coupling-induced distortions of tune-footprint have the potential to affect Landau damping of instabilities. In 2016 this was explicitly demonstrated in the LHC, with beam- and simulation-based studies attesting to a substantial destabilizing effect on LHC beams from the introduction of linear coupling [31, 32]. During luminosity production the LHC operates with crossing-angle orbit bumps in the experimental insertions. As a consequence of these bumps, IR-nonlinear errors can generate substantial feed-down to linear coupling. While such feed-down could in principle be corrected globally for a specific optics and crossing scheme, introduction of crossing-angle levelling and β^*-levelling into regular LHC operation, as well as the routine manipulations of IR-orbit bumps during machine studies, gave significant motivation for compensation of the relevant multipole errors.

Feed-down arising from crossing-angles in the experimental insertions will not only perturb linear coupling, but also the linear optics. While the beta-beat generated through feed-down in the IRs was not expected to be critical to LHC operation at $0.4\,\mathrm{m}$ [22], it has been clearly demonstrated in previous years that improvements to linear optics quality have a positive influence on a broad range a machine parameters [6]. Furthermore, any potential source of luminosity imbalance between the ATLAS and CMS experiments is of great concern. In all previous years, commissioning of linear optics in the LHC has

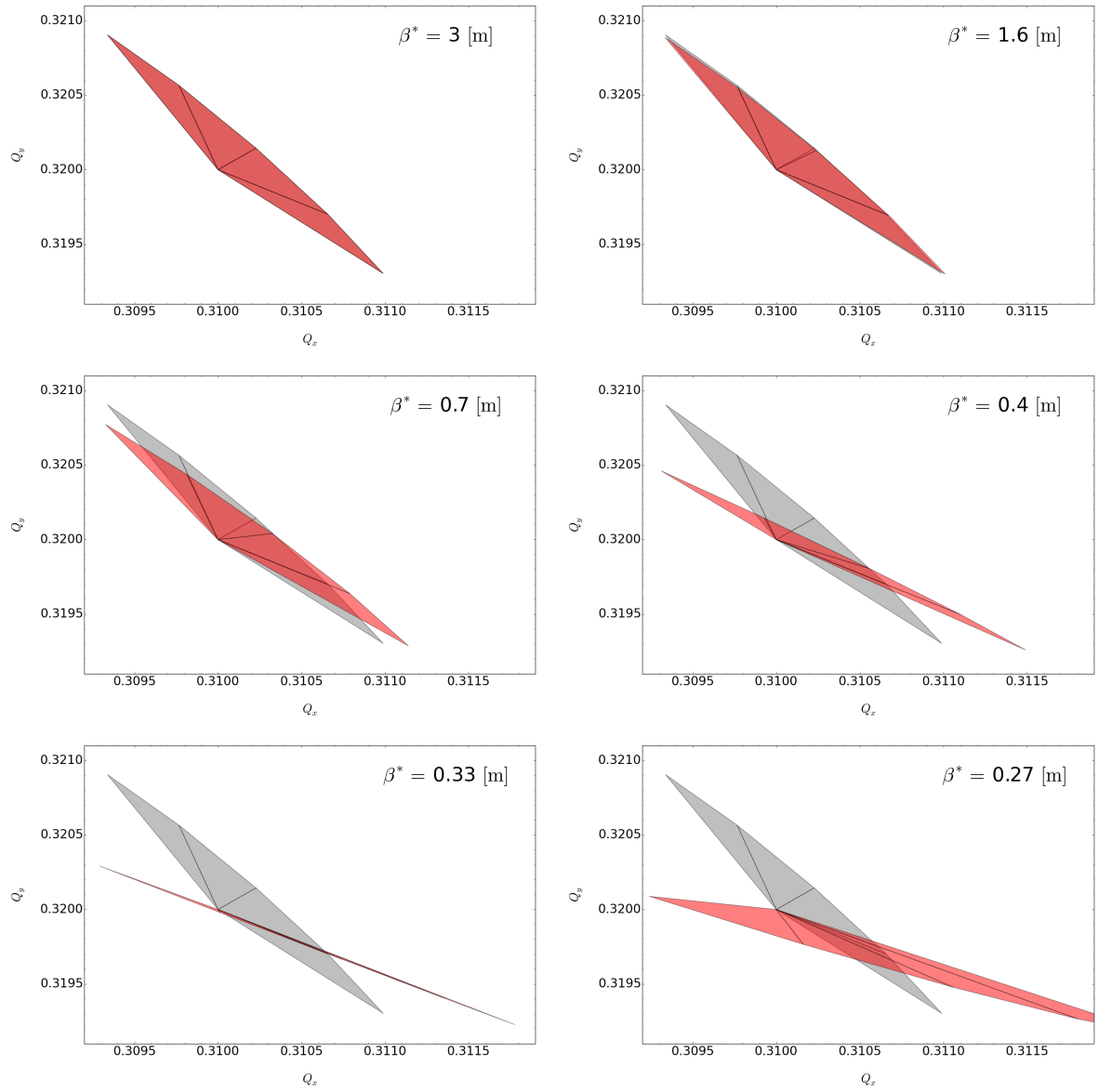

Fig. 1: Distortion of tune-footprint through the β^* squeeze. Displayed footprints are defined by first-order detuning coefficients obtained via simulation. Simulations consist of an effective model of normal octupole errors in IR1 and IR5, which reproduces the observed detuning at $\beta^* = 0.4\,\mathrm{m}$ and $0.6\,\mathrm{m}$, together with Landau octupoles powered as per operation for luminosity production in late 2016. Grey regions show the desired footprint, expected in the absence of the IR contribution Red regions show the inferred footprint in the real LHC, if IR octupole errors are left uncompensated.

been performed at flat-orbit (a closed-orbit without any orbit bumps in the experimental IRs). In 2017, to ensure the smallest possible β^*-imbalance between the HEP experiments, not only was it decided to attempt direct correction of the nonlinear sources in the IRs, but also to perform a linear re-optimization of the optics at the operational crossing scheme after all higher-order corrections were applied.

For the first time, the LHC now operates with dedicated corrections for nonlinear errors in its low-β^* insertions, and for the impact of the operational crossing-scheme on the linear optics. This paper reports the results of the first combined linear and nonlinear optics commissioning of the LHC. Section 2 describes an initial linear optics commissioning at flat-orbit. Section 3 describes the methodology and

Table 1: Local linear optics corrections in the LHC experimental insertions. Magnets are defined such that 'Q1' is the innermost triplet on the left or right side of the IR, while 'Q3' is the outermost (see Fig. 7). Absolute values of the correction strengths are shown, together with the percentage of the correction relative to magnet powering at $\beta^* = 0.4\,\mathrm{m}$

Magnet	ΔK_2		Magnet	ΔK_2	
	$[10^{-5}\mathrm{m}^{-2}]$	[%]		$[10^{-5}\mathrm{m}^{-2}]$	[%]
Q1 L1	1.23	−0.14	Q1 L5	2.00	−0.23
Q1 R1	−1.23	−0.14	Q1 R5	−2.00	−0.23
Q2 L1	0.65	0.07	Q2 L5	0.26	0.03
Q2 R1	−1.00	0.11	Q2 R5	1.58	−0.18
Q3 L1	1.22	−0.14	Q3 L5	1.49	−0.17
Q3 R1	−1.22	−0.14	Q3 R5	−1.49	−0.17
Q2 L2	−1.50	0.17	Q2 L8	−1.00	0.11
Q2 R2	1.50	0.17	Q2 R8	–	–

results of the first nonlinear commissioning of the LHC. Finally Section 4 will report on the first linear optics commissioning of the LHC at the operational crossing scheme, and present results for the final optics quality.

2 Linear optics commissioning with a flat orbit

Prior to 2017, linear optics commissioning in the LHC was performed exclusively with a flat closed-orbit. In 2017 linear optics commissioning was also initially performed at flat-orbit, in order to establish a baseline linear optics in good agreement with the nominal model used for calculation of nonlinear optics corrections. Measurement of the linear optics is generally based upon K-modulation and spectral analysis of turn-by-turn (TbT) beam position monitor (BPM) data of driven oscillations generated by an AC-dipole. Linear optics can be corrected through direct constraint of the measured phase advances between BPMs, while β-beating is inferred from said phase advances utilizing the N-BPM method [3]. Dispersion is not corrected directly, but rather through constraint of normalized dispersion ($D_x/\sqrt{\beta}$), which is independent of BPM calibration errors [33]. Between 2012 and 2016 low-β^* optics commissioning was performed in two stages: with initial corrections for local errors in the insertions applied to the virgin machine (a machine configuration with all beam-based corrections removed), followed by simultaneous global optimization of β^*, betatron phase advances around the ring, and normalized dispersion. Detailed descriptions of the methods used in LHC linear optics commissioning may be found in [1–7, 33, 34]. An overview of these methods, within the broader context of optics measurement techniques, may be found in [35].

Commissioning of the operational LHC optics in 2016 yielded excellent results following the procedure described above [7], and in preparation for the transition to Achromatic Telescopic Squeeze (ATS) optics [36, 37] the ATS linear optics scheme was successfully commissioned to $\beta^* = 0.4\,\mathrm{m}$ and below during dedicated machine development studies in 2016 [38]. To reduce the time required for optics correction, the 2017 commissioning started with local corrections determined the previous year already applied (see Tab. 1). As in previous years the local corrections were aproximately double the anticipated value, based upon the expected magnetic errors [7]. A slight degradation of the local optics correction quality developed between 2016 and 2017. This can be seen in Fig. 2, which compares the deviation from nominal phase advance between BPMs in IR5 (measured via the segment-by-segment technique [1]) in 2016, to that measured in 2017 with the old corrections applied.

The effect of local optics degradation in the IRs can also be seen in Figs. 3 and 4 (red). Clear jumps

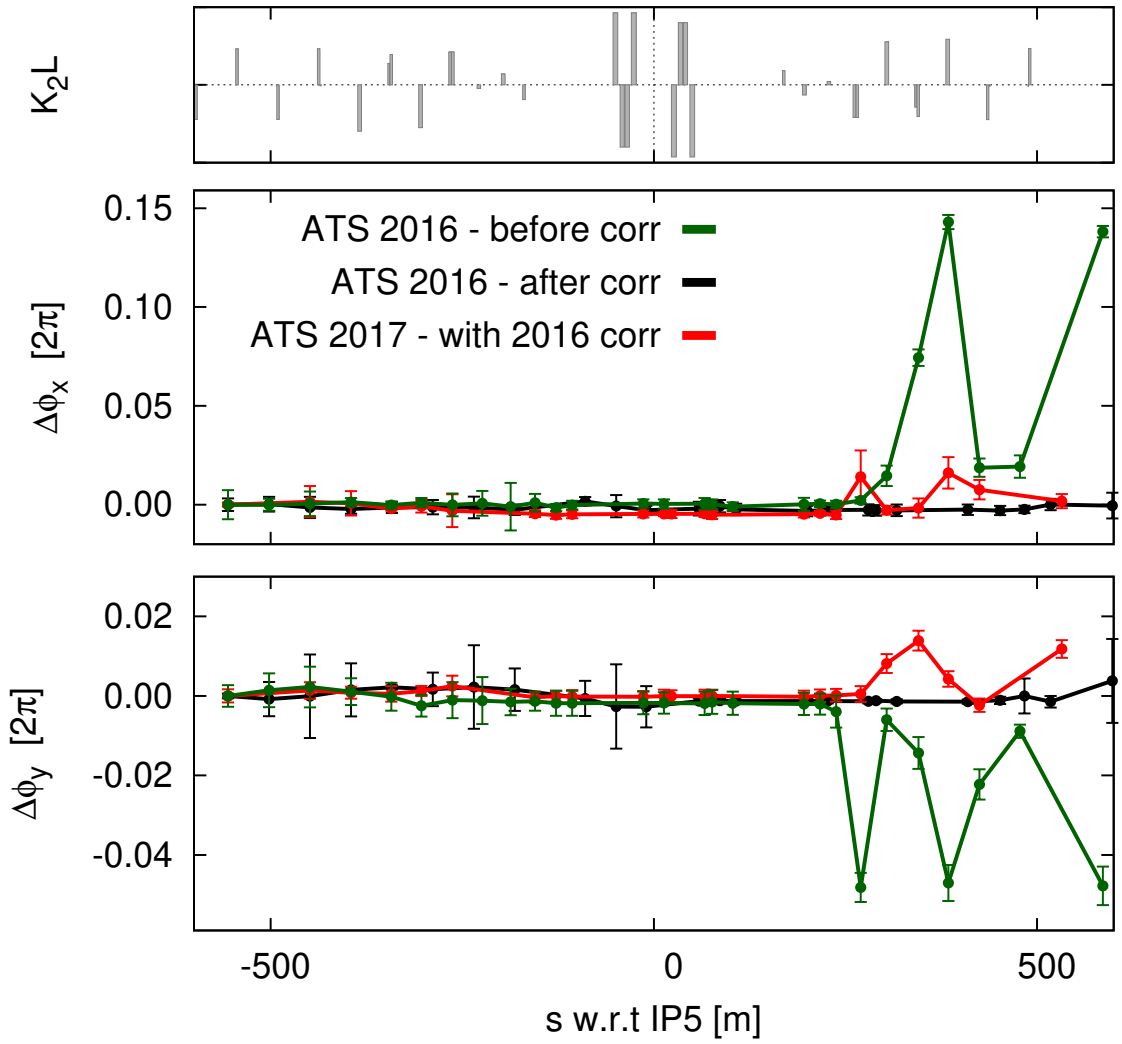

Fig. 2: Propagated phase error through IR5. Measurements for ATS optics in 2016 are shown before correction (green) and after correction (black). The optics quality obtained in 2017, with the 2016 correction applied, is shown in red.

in β-beat are seen to originate in the insertions. In spite of this, the optics quality obtained using the old settings was considered sufficient to proceed without further iteration of the local correction, and global optimization was performed. The measured beta-beat after global correction is shown in Figs. 3 and 4 (blue). Figure 5 compares normalized dispersion before and after global correction, which is seen to significantly reduce residual local errors in the insertion regions. Table 2 compares optics quality at $\beta^* = 0.4\,\mathrm{m}$, obtained in 2017 with ATS optics, to that obtained in 2016 with nominal optics. A slight deterioration (at the level of $\sim 1\,\%$) can be seen to remain in the post-correction RMS β-beat of the horizontal plane, likely a consequence of not re-iterating the local corrections between the two years. Peak values in 2017 appear slightly worse than 2016, but are dominated by a minority of outlying BPMs. It is unclear whether these outlying measurements are a consequence of the uncompensated local errors in the IRs (Beam 2 for example shows several BPMs around IR1 and IR5 at a horizontal β-beat several times greater than the RMS value), or the result of a few poorly reconstructed BPM measurements. Nonetheless, in spite of the degradation to the local corrections, linear optics quality for the ATS scheme at flat-orbit is comparable to that obtained for the nominal LHC optics in previous years [5–7].

Linear coupling in the LHC is compensated by minimization of the f_{1001} resonance driving term

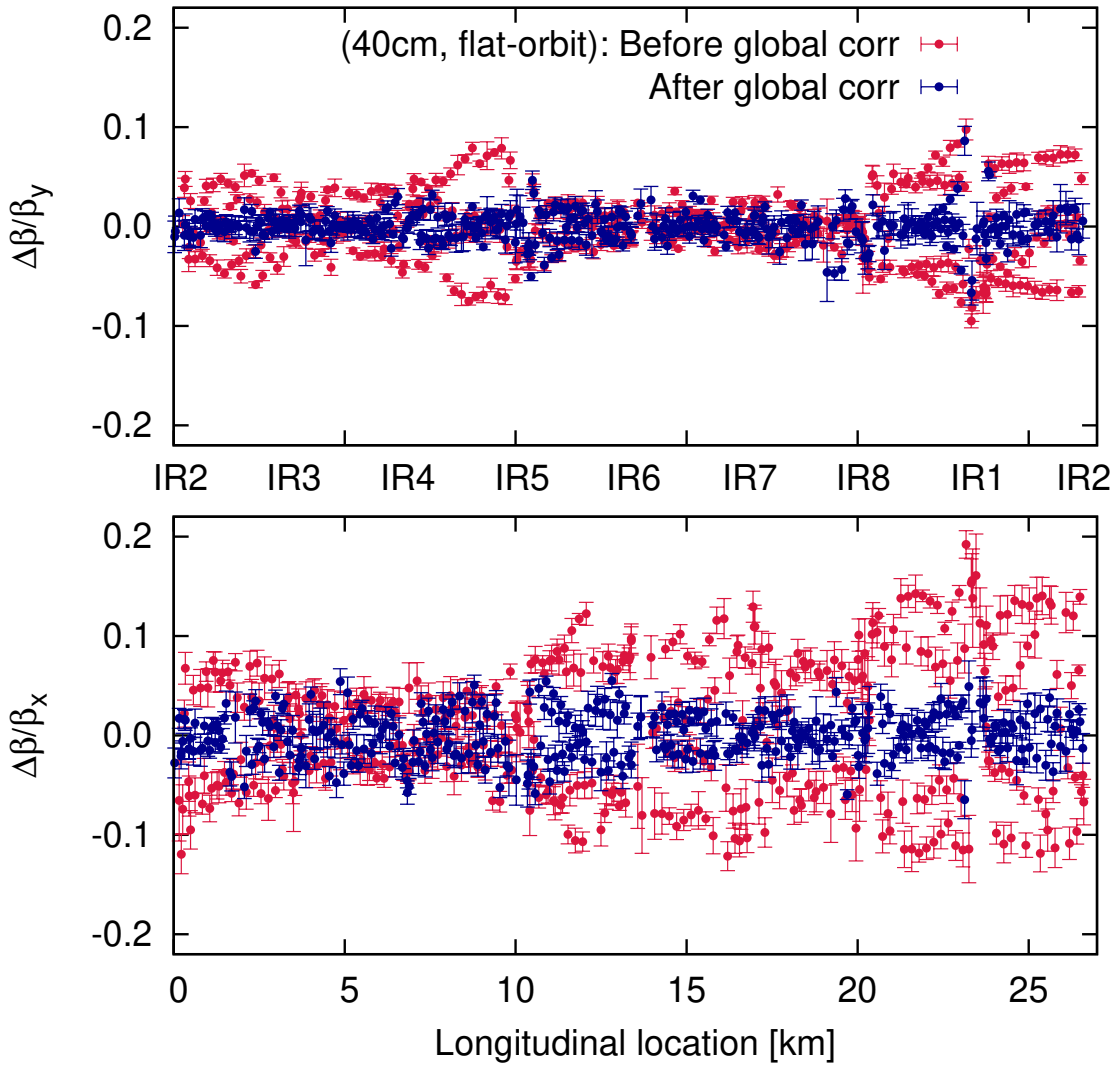

Fig. 3: β-beat in LHC Beam 1 before and after application of global optics correction at flat-orbit in 2017.

Table 2: Comparison of linear optics quality obtained with flat-orbit for the 2017 ATS optics at $\beta^* = 0.4\,\mathrm{m}$, to that obtained with flat-orbit in 2016 for the nominal $0.4\,\mathrm{m}$ optics. Values for 2016 were taken from [7].

	2017 ATS		2016 Nominal	
	Beam 1	Beam 2	Beam 1	Beam 2
$\beta_x\|_{\mathrm{RMS}}$ [%]	2.3	2.6	1.4	1.4
$\beta_y\|_{\mathrm{RMS}}$ [%]	1.5	1.5	1.8	1.4
$\beta_x\|_{\mathrm{peak}}$ [%]	5.5	10.9	7.7	4.5
$\beta_y\|_{\mathrm{peak}}$ [%]	8.6	7.6	5.8	4.9
$\frac{\Delta D_x}{\sqrt{\beta_x}}\|_{\mathrm{RMS}}$ $[10^{-2}\mathrm{m}^{-\frac{1}{2}}]$	0.45	0.58	0.52	0.62
$\lvert\frac{\Delta D_x}{\sqrt{\beta_x}}\rvert_{\mathrm{peak}}$ $[10^{-2}\mathrm{m}^{-\frac{1}{2}}]$	1.2	4.3	1.9	1.8

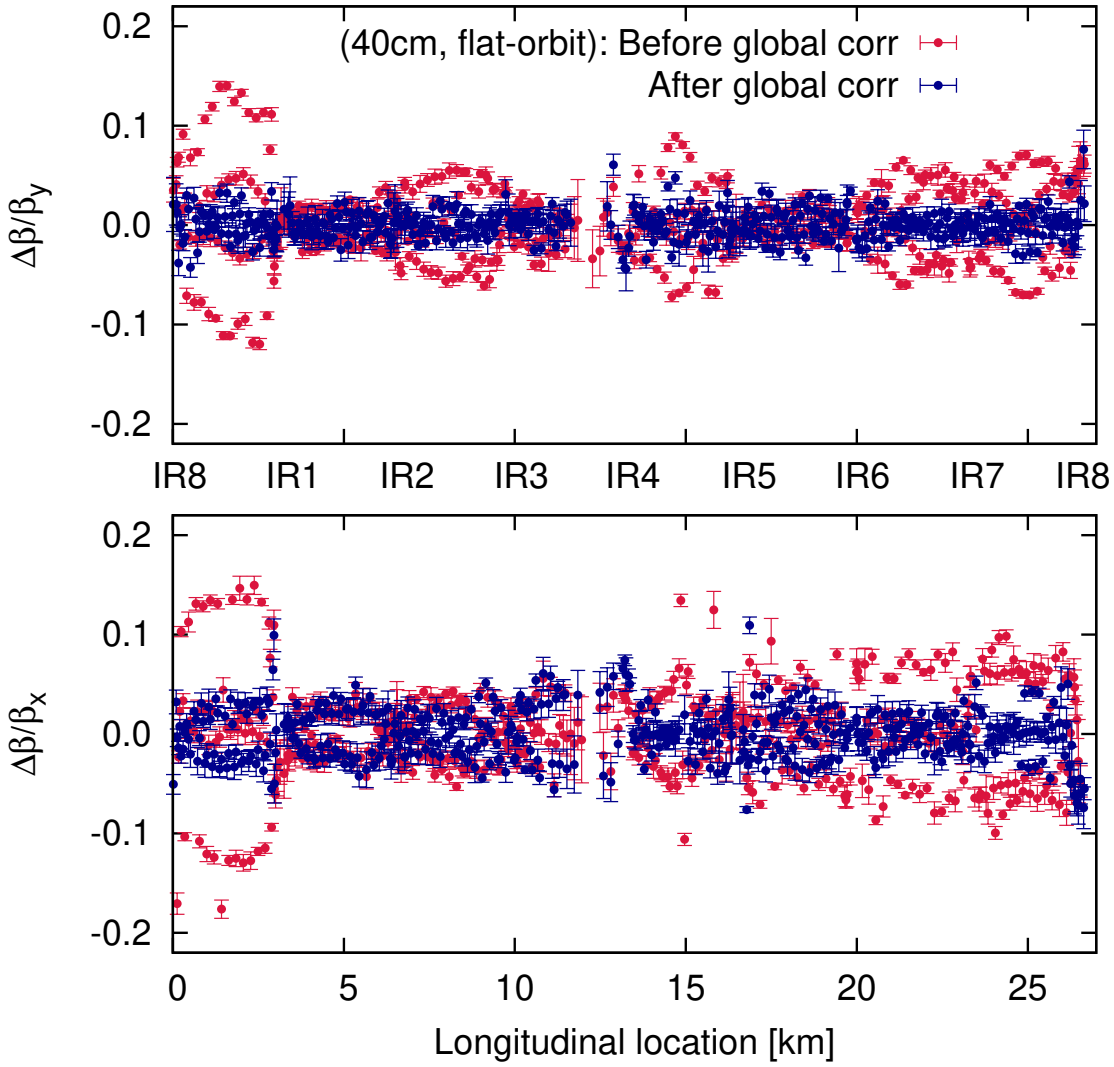

Fig. 4: β-beat in LHC Beam 2 before and after application of global optics correction at flat-orbit in 2017.

(RDT), related to the $(Q_x - Q_y)$ coupling resonance, and measured via spectral analysis of TbT BPM data for driven oscillations with an AC-dipole. Description of the relevant theory and correction techniques may be found in [6, 7, 39–41]. In the LHC, correction of f_{1001} has allowed values of the linear coupling as low as $|C^-| = 2 \times 10^{-4}$ to be achieved in dedicated tests [42], with typical operational values of the order of 10^{-3}. Experience in 2016 has demonstrated the importance of linear coupling to a wide range of linear and nonlinear phenomena [26, 31, 32]. In 2017 coupling was corrected throughout the LHC cycle, with an ultimate correction quality consistent with that obtained in previous years [7, 43]. Given the growing appreciation of the importance coupling holds to LHC operation however, it was decided to extend commissioning strategy to include compensation of chromatic coupling.

Chromatic coupling refers to a momentum dependent linear coupling. A first-order dependence of linear coupling on the relative momentum offset can be generated by skew sextupole sources in regions of horizontal dispersion, and normal sextupoles in regions of vertical dispersion. At flat-orbit these sources lie primarily in the LHC arcs. Chromatic coupling is measured via AC-dipole excitation at varying momentum offset, yielding the change in f_{1001} as a function of $\delta p/p$. It is compensated via skew sextupole correctors located in the arcs. Measurement and correction of chromatic coupling was demonstrated in the LHC during dedicated studies in Run 1 [44], however compensation was never before implemented operationally.

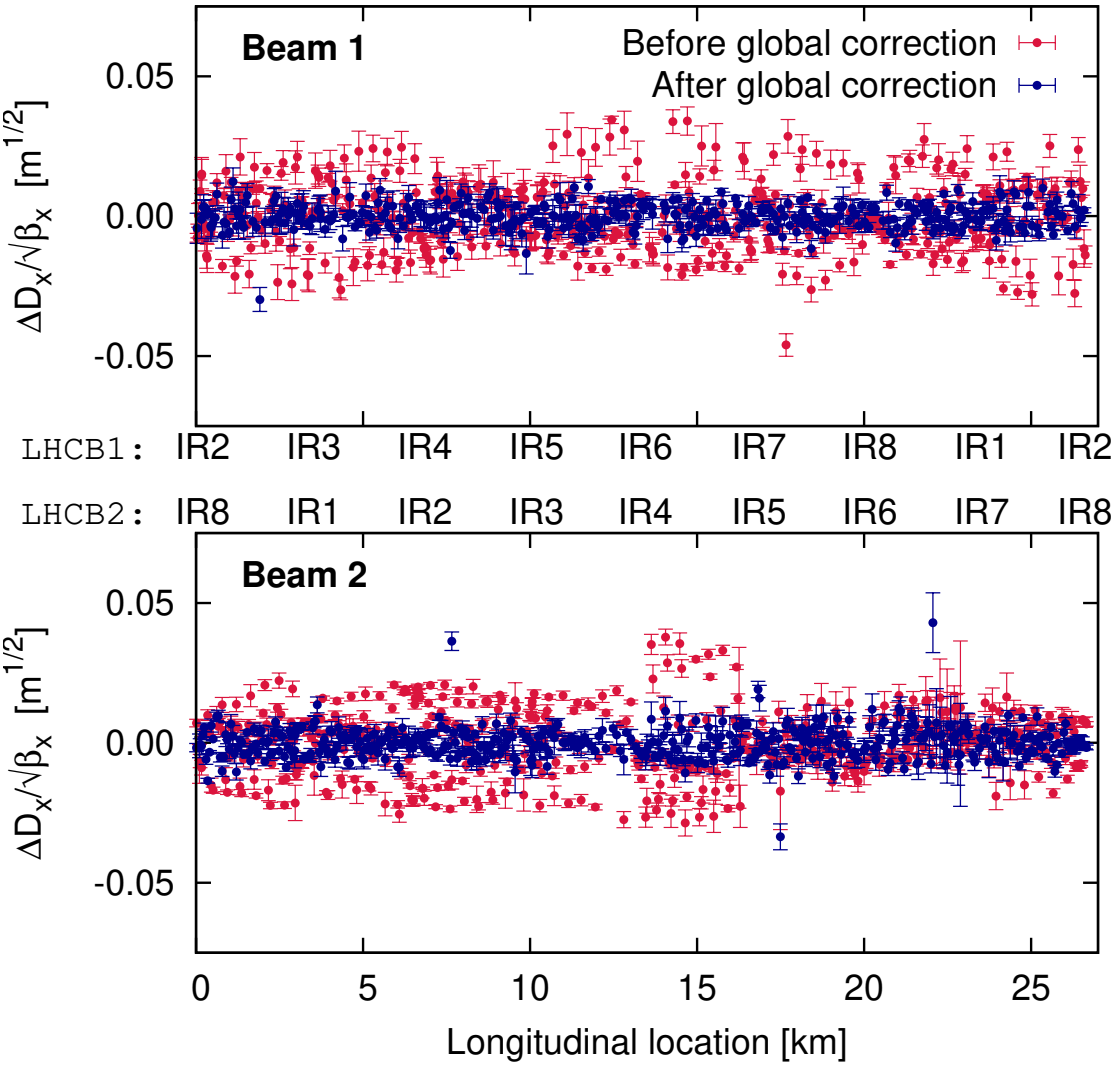

Fig. 5: Normalized dispersion at flat-orbit for LHC Beam 1 (top) and LHC Beam 2 (bottom), before and after application of global optics corrections in 2017.

Figure 6 (red) shows the chromatic coupling measured after application of global optics corrections, but before any skew sextupole correction was applied. Chromatic coupling was found to be particularly large in Beam 2, where for a particle with relative momentum offset $\frac{\delta p}{p} = 10^{-4}$ the observed value is approximately equivalent to $\Delta|C^-| \approx 0.001$. The nominal RMS momentum spread of LHC bunches is 10^{-4} at top energy, while chromaticity ($Q'_{x,y}$) measurements typically utilize RF modulation of $\frac{\delta p}{p} = \pm 2 \times 10^{-4}$. Corresponding $\Delta|C^-|$ from synchrotron motion and Q' measurements are thus comparable with typical on-momentum values of the linear coupling, potentially leading to operationally relevant effects in regard to control of chromaticity and Landau damping. After correction of the chromatic coupling (Fig. 6, blue) the variation of $|C^-|$ with relative momentum offset was reduced to levels of negligible significance in both beams. For the first time the LHC now operates with chromatic coupling compensated.

3 Commissioning of the nonlinear optics

Dedicated correctors are located on the left and right sides of each experimental IR, explicitly for the purpose of locally compensating nonlinear errors. Correctors are available for normal and skew sex-

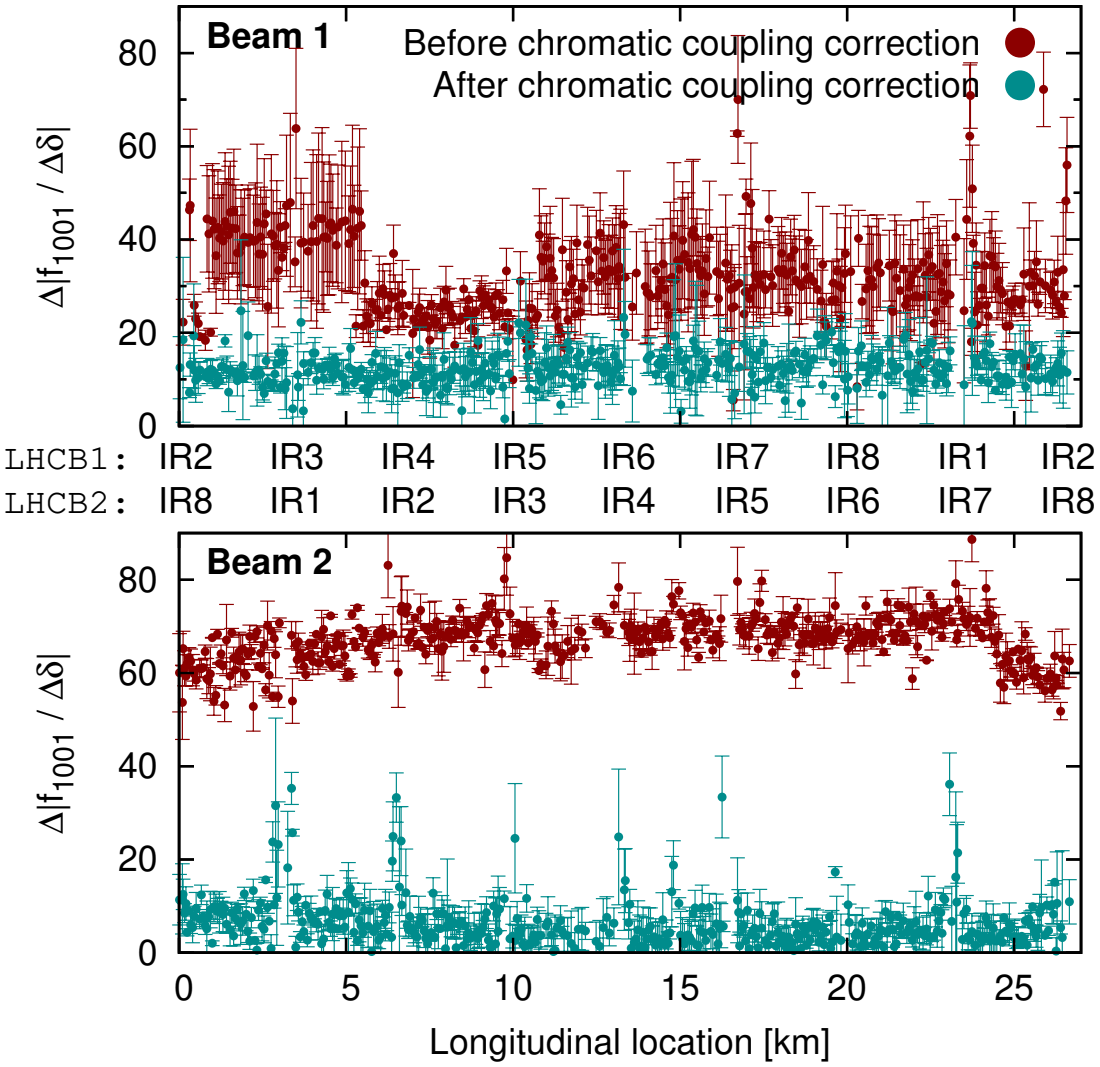

Fig. 6: Measurements of chromatic coupling before (red) and after (blue) compensation with skew sextupole correctors in the LHC arcs. Plots are shown for Beam 1 (top) and Beam 2 (bottom).

tupole, normal and skew octupole, and normal dodecapole multipoles. All correctors may be powered independently, however as they are located in the region of common aperture the two LHC beams cannot be corrected independently. Since the errors also lie in the region of common aperture however, common local correction of the two beams should in general be viable. Figure 7 displays a schematic of one side of an LHC experimental IR. The nonlinear correctors are located on the non-IP side of the Q3 triplet quadrupole (location C3 in Fig. 7). Further details regarding the lattice and the corrector magnets may be found in [10, 45]. Prior to 2017 nonlinear correctors in the experimental IRs had never been used in LHC operation.

During LHC design it was assumed that nonlinear corrections in the IRs would be determined from magnetic measurements performed during construction. These measurements would allow optimal corrections for specific resonance driving terms (RDTs) to be calculated analytically as described in [46, 47]. In 2011 and 2012 beam-based studies of feed-down from the nonlinear errors in LHC IRs were performed. Comparison of these beam-based studies, to the prediction of models incorporating the magnetic measurements, demonstrated that for several of the multipole orders discrepancies existed between the magnetically measured multipole errors and those seen by the LHC beams [48]. This result precluded straightforward application of the design strategy. Consequently greater emphasis has been

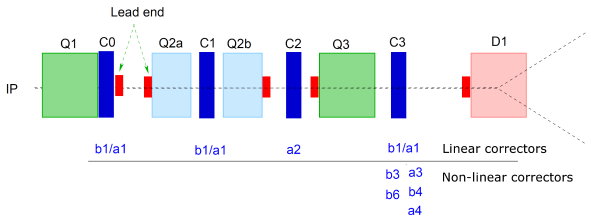

Fig. 7: Linear and nonlinear corrector layout in LHC experimental IRs [46].

placed on the beam-based study of IR-nonlinearities in recent years.

During the LHC's second operational run, considerable effort was invested into the development of new methodologies for the study of nonlinear errors in low-β^* IRs. Theoretical developments in understanding the influence of driven oscillations on action-dependent tune shifts [21] enabled AC-dipole based measurements of amplitude detuning at $6.5\,\mathrm{TeV}$. This provided an additional observable which had previously been impossible to probe at top energy using conventional measurements based upon single-kicks and free oscillations. In parallel, an improved understanding of dynamic aperture in the presence of such driven oscillations helped avoid the limitation of nonlinear optics studies by chaotic beam-losses [49, 50]. The repertoire of available measurements was also expanded to include study of resonance driving terms, with some RDTs up to octupolar order shown to be observed in dedicated tests [51, 52]. Existing techniques based upon feed-down were also refined. Active control of orbit-leakage significantly improved the validity of measurements based upon orbit scans in the IRs [51], while a shift from online measurement of $|C^-|$ with the LHC Base-Band Tune (BBQ) system [53, 54] to direct measurement of linear coupling RDTs using an AC-dipole provided a more robust observable for feed-down to linear coupling [51].

In the nominal correction strategy for the LHC it was assumed that nonlinear corrections in the experimental IRs would be based upon compensation of specific RDTs [46]. As will be seen in the following sections however, this has not generally proved to be the case. Measurement of high-order RDTs is challenging, with relevant spectral lines often lying close to the noise floor of the betatron tune spectrum, and to facilitate the nominal correction strategy the local variations of several RDTs from any given multipole would need to be measurable. Analysis is also challenging since kicker limitations in the LHC mean RDT measurements need to be performed via AC-dipole excitation. RDTs measured by forced oscillations actually correspond to a mixture of resonances of the free motion [55] creating ambiguity in the specific resonance being studied. As AC-dipole RDTs (labelled f'_{jklm} as opposed to f_{jklm}) do not mix resonances from different multipole species however, the driven RDTs do still provide a good observable for multipole strength more generally. Finally, simulation-based studies of the LHC and HL-LHC have indicated that the direct impact of a given multipole order may not always be the most operationally relevant feature of the dynamics. Loss of Landau damping during crossing-angle levelling, due to feed-down from nonlinear errors to linear coupling for example, can prove to be a more significant risk to operation than the corresponding resonances.

Considerable work has been invested into developing methodology to study and compensate resonance driving terms in the LHC, the details of which lie outside the scope of this publication but can be found in [52, 55, 56]. Rather than relying only on RDTs for correction of nonlinear errors in the LHC low-β^* IRs as originally envisaged however, a broad range of beam-based observables have been utilized instead. For the initial venture into nonlinear optics commissioning of the LHC reported here, beam-based corrections were in the main calculated based upon measurements of amplitude detuning, and feed-down to either linear coupling or tune. While RDT measurements were performed, they were used exclusively in the role of validation of corrections calculated by other means.

Regarding the nonlinear corrections, since correctors are only mounted at a single location left and

right of the IR (while β-ratios and closed orbit will vary over every element in the IR) any correction of the nonlinearities within the insertion will be quasi-local. Corrections based upon one observable, for example feed-down, may then differ from direct RDT correction. According to [46] correction of the RDTs may be performed by powering the corrector magnets to minimize the integral:

$$\begin{aligned} &\int_{IR} \mathrm{d}s\, K_n(s)\, \beta_x^{\frac{j+k}{2}} \beta_y^{\frac{l+m}{2}} e^{\pm i\left[(j-k)\phi_x \pm (l-m)\phi_y\right]} \\ \approx &\int_{IR_{\text{left}}} \mathrm{d}s\, K_n(s)\, \beta_x^{\frac{j+k}{2}} \beta_y^{\frac{l+m}{2}} + (-1)^n \int_{IR_{\text{right}}} \mathrm{d}s\, K_n(s)\, \beta_x^{\frac{j+k}{2}} \beta_y^{\frac{l+m}{2}} \\ &\text{where} \quad n = j+k+l+m \end{aligned} \tag{1}$$

where K_n is the multipole strength in $[\mathrm{m}^{-\mathrm{n}}]$ (with $n = 2$ denoting a quadrupole, $n = 3$ a sextupole, etc.) and the latter approximation assumes a π phase advance between the left and right sides of the IR, with negligible phase advance on either side of the insertion. In contrast, correction of feed-down could be achieved through minimization of an integral resembling:

$$\int_{IR} \mathrm{d}s\, \Re e \left[\frac{(\Delta x)^q}{q!(n-q)!} \left(K_n + iK_n^{(s)} \right) \sum_{p=0}^{n-q} i^p \binom{n-q}{p} x^{(n-p-q)} y^p \right] = \tag{2}$$

$$= \int_{IR} \mathrm{d}s\, \Re e \left[\frac{(\Delta x)^q}{q!(n-q)!} \left(K_n + iK_n^{(s)} \right) \sum_{p=0}^{n-q} i^p \binom{n-q}{p} \beta_x^{\frac{n-p-q}{2}} \beta_y^{\frac{p}{2}} \left(\sqrt{2J_x} \cos\phi_x \right)^{(n-p-q)} \left(\sqrt{2J_y} \cos\phi_y \right)^p \right]$$

$$\propto \int_{IR} \mathrm{d}s\, \Delta x\,(s)^q\, K_n(s)\, \beta_x^{\frac{n-p-q}{2}} \beta_y^{\frac{p}{2}} \equiv \int_{IR} \mathrm{d}s\, \Delta x\,(s)^q\, K_n(s)\, \beta_x^{\frac{j+k-q}{2}} \beta_y^{\frac{l+m}{2}}$$

$$\text{with } j+k+l+m = n \text{ and } l+m \le n-q \le j+k$$

for the specific case of a horizontal offset through the IR. Once again n defines multipole order, while p defines the specific monomial of the Hamiltonian in question, and q defines the order of the feed-down (thus $q = 2$ would correspond to feed-down from an octupole to quadrupole, or from dodecapole to octupole). In practice the specific monomial considered and the $J_{x,y}$ dependence are a consequence of the observable(s) selected. For feed-down to tune from a sextupole for example, one could attempt to power sextupole correctors in order to minimize:

$$\begin{aligned} \Delta Q_{x,y} &\approx \frac{1}{2\pi} \left\langle \frac{\partial H}{\partial J_{x,y}} \right\rangle_{\phi_{x,y}} \\ &\xrightarrow[\text{via Eq. (2)}]{} \pm \int_{IR} \mathrm{d}s \frac{1}{4\pi} \Delta x(s)\, \beta_{x,y}(s)\, K_3(s) \end{aligned} \tag{3}$$

Compared to Eq. 1, corrections based upon feed-down will feature different weightings of the sources with $\beta_{x,y}$, as well as on the beam-offset through the error/corrector. Providing the applied corrections are still approximately local however, corrections based upon feed-down from the crossing-angle orbit bumps should still reduce other observables such as RDTs (and vice versa). Although they may not represent the optimal correction of those alternative parameters.

Commissioning for the nonlinear errors in the LHC began with correction of normal octupole sources in the ATLAS and CMS insertions, described in Sec. 3.1, since minimizing amplitude detuning early in the commissioning period is beneficial to both the linear and lower-order nonlinear measurements and corrections. Simultaneous corrections were then applied for normal sextupole errors in the CMS insertion, and for normal sextupole, skew sextupole, and skew octupole errors in the ATLAS insertion. Sextupole correction in IR5 is discussed in Sec. 3.2, while the sextupole and skew octupole corrections in IR1 are discussed in Sec. 3.3.

3.1 Normal octupole correction in the ATLAS and CMS insertions

Of foremost concern for LHC operation in 2017 was compensation of normal octupole errors in IR1 and IR5. First-order amplitude detuning, a linear variation of tune with particle action ($J_{x,y}$), relates directly to the integrated octupole content of the machine, weighted by $\beta_{x,y}^2$ at the octupoles. At small β^*, with Landau octupoles depowered, amplitude detuning in the LHC is dominated by the contribution from IR1 and IR5. Figure 8 shows amplitude detuning of LHC Beam 2, measured with an AC-dipole at $\beta^* = 0.4\,\mathrm{m}$ (flat-orbit) in 2016. This is compared to MAD-X/PTC [57, 58] predictions in gray, for models including the measured magnetic errors. Predictions are adjusted for the impact of driven oscillations with an AC-dipole [21]. Similar results were obtained for LHC Beam 1.

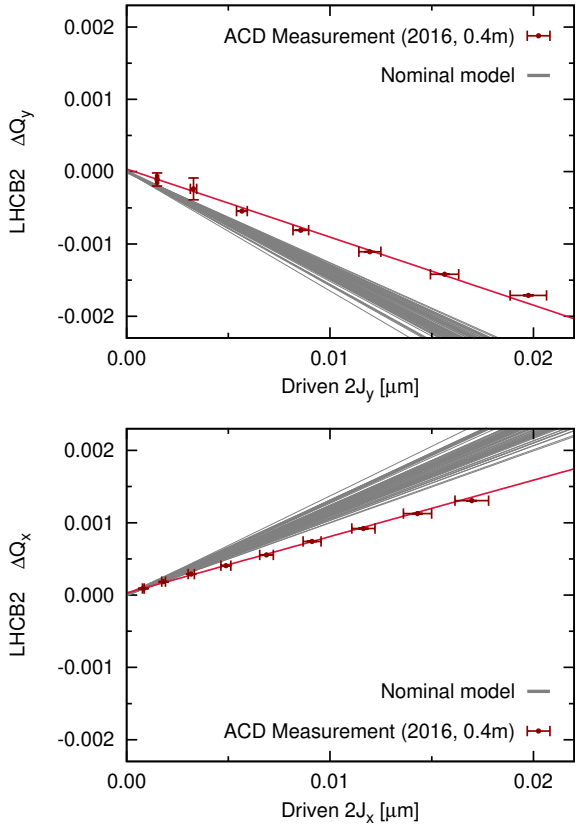

Fig. 8: Amplitude detuning measured with flat-orbit in 2016, for LHC Beam 2 at $\beta^* = 0.4\,\mathrm{m}$ with MO powered off (red). Simulated detuning is shown in gray, for models based upon the measured magnetic errors. Sixty instances of the magnetic errors are simulated, corresponding to the uncertainty in the magnetic measurements.

Cross-term detuning, $\frac{\partial Q_x}{\partial \epsilon_y} = \frac{\partial Q_y}{\partial \epsilon_x}$, (where $\epsilon_{x,y} = 2J_{x,y}$) was consistent with zero within measurement errors as expected from the LHC magnetic model. It is not shown in Fig. 8. Direct terms ($\frac{\partial Q_x}{\partial \epsilon_x}$ and $\frac{\partial Q_y}{\partial \epsilon_y}$) however, showed a $\sim 30\,\%$ discrepancy relative to that expected from the magnetic measurements. On their own, these measurements cannot be used to determine corrections for IR-b_4, as it is impossible to distinguish sources in IP1 and IP5. In 2012 however, when comparing measurements of feed-down to tune as a function of crossing-angle in IP1, it was found that the quadratic tune shift ($\Delta Q \propto y^2$, dependent on IR-octupole errors) showed a good agreement with predictions of the magnetic model [48]. Measurements in 2015 and 2016 also demonstrated a good agreement of second-order tune feed-down in IR1. An example is shown in Fig. 9, for measurement of Q_y as a function of the vertical crossing-angle at IP1 in 2015. In contrast quadratic variation of tune as a function of crossing-angle in IR5 showed substantial discrepancies with the predictions of the magnetic model [48].

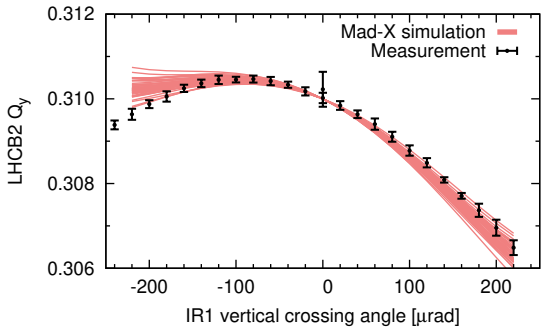

Fig. 9: Measured tune (black) as a function of the vertical crossing-angle in the ATLAS insertion, compared to predictions based upon magnetic measurements (red).

Combining amplitude detuning and feed-down data, a correction strategy for normal octupole errors in the ATLAS and CMS insertions could be devised. Given the close agreement to model predictions, IR1 corrections were calculated directly from the magnetic measurements following the procedure in [46]. Normal octupole correctors left and right of IP5 were then matched in simulation, to minimize the residual detuning expected for both beams after application of the IR1 correction. The normal octupole correction for IR1/5 was applied at the very beginning of low-β^* optics commissioning in 2017, even before global correction of the linear optics at $0.4\,\mathrm{m}$. Figure 10 shows the applied beam-based corrections left and right of IR1 and IR5, compared to the corrections expected from the magnetic measurements. The discrepancy with the magnetic model remains unexplained, though feed-down from decapole or dodecapole errors arising from alignment errors in the IRs appears one potential source [59], and it has not proved possible to find corrections to re-balance the correction between IR1 and IR5 without deteriorating either feed-down or amplitude detuning.

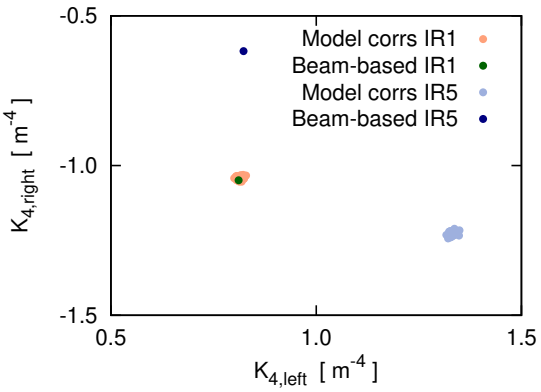

Fig. 10: Beam-based corrections for the normal octupole errors applied in the ATLAS and CMS insertions, compared to the expected corrections based upon magnetic measurements. Sixty instances of the model-based corrections are shown, corresponding to the uncertainty in the magnetic measurements.

A beneficial effect from this correction was seen immediately, through a clear improvement in the performance of beam-instrumentation. Figure 11 shows an example of substantial reduction in noise in the online tune measurement, obtained upon application of the normal octupole correction.

A clear influence was also observed in the online measurement of linear coupling via the LHC BBQ system. A substantial reduction ($\Delta|C^-| \approx 4 \times 10^{-3}$) can be seen in Fig. 12 upon application of the b_4 correction.

It should be emphasised that the coupling shift observed in Fig. 12 is not real. In 2012 it was observed that the LHC BBQ displayed impossibly large coupling shifts upon changes in octupole power-

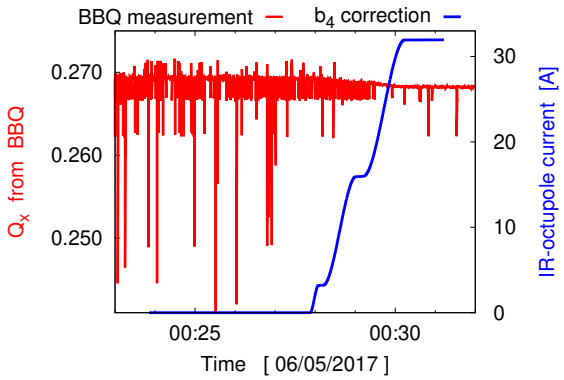

Fig. 11: Improvement in online tune measurement quality upon application of corrections for normal octupole errors in the ATLAS and CMS insertions.

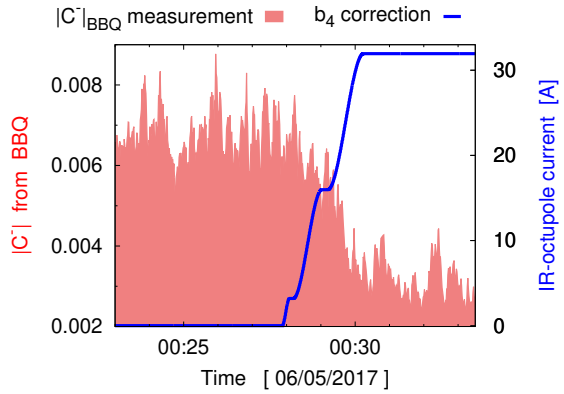

Fig. 12: Improvement in online coupling measurement upon application of normal octupole corrections in the ATLAS and CMS insertions.

ing [60], incompatible with more reliable measurements, and online measurement of $|C^-|$ could only be trusted in the absence of strong octupolar sources [61] (including in the IRs). This artifact was demonstrated to arise from changes in the noise-to-signal ratio of coupling lines in the BBQ spectrum, due to increased tune-spread generated by octupoles [62]. The apparent shift in Fig. 12 corresponds to an improved reliability of the BBQ, due to a reduction in tune-spread upon application of the IR-b_4 corrections. Indeed, after IR-octupole correction the $|C^-|$ recorded by the BBQ was found to be consistent with that measured via the more reliable AC-dipole technique ($|C^-|_{\mathrm{AC-dipole}} = 0.0028$), facilitating continuous $|C^-|$ measurement during the squeeze.

The improved BBQ performance obtained upon application of normal octupole corrections was of significant assistance to LHC operation in 2017. Within the context of LHC optics commissioning, this improved BBQ performance was also considered fundamental to obtain high quality K-modulation data at $\beta^* = 0.4$ and $0.3\,\mathrm{m}$, facilitating control of the β^* imbalance between the ATLAS and CMS experiments. The observation also provided a qualitative validation of the b_4 correction, which remained in place throughout commissioning and operation in 2017.

Direct confirmation of the b_4 correction was performed at the end of the commissioning period, at a β^* of $0.3\,\mathrm{m}$. Figure 13 shows a comparison of the amplitude detuning measured with AC-dipole in 2017 at $\beta^* = 0.3\,\mathrm{m}$ after normal octupole correction in IR1 and IR5, to that measured in 2016 at $\beta^* = 0.4\,\mathrm{m}$ before correction. Due to a reduced physical aperture at $\beta^* = 0.3\,\mathrm{m}$, and larger emittance beams in 2017, the amplitude range probed after correction is significantly smaller than was possible in 2016. By combining AC-dipole measurements with BBQ data for the unperturbed tune however, it

Table 3: Amplitude detuning coefficients at $\beta^* = 0.4\,\mathrm{m}$ without IR-b_4 correction, and at $\beta^* = 0.3\,\mathrm{m}$ after correction.

Detuning coefficients $[10^3\,\mathrm{m}^{-1}]$		$\beta^* = 0.4\,\mathrm{m}$ (no correction)	$\beta^* = 0.3\,\mathrm{m}$ (with correction)
LHCB1	$\frac{\partial Q_x}{\partial \epsilon_x}$	43 ± 1	-3 ± 1
	$\frac{\partial Q_x}{\partial \epsilon_y} = \frac{\partial Q_y}{\partial \epsilon_x}$	0 ± 1	5 ± 3
	$\frac{\partial Q_y}{\partial \epsilon_y}$	-50 ± 1	No measurement
LHCB2	$\frac{\partial Q_x}{\partial \epsilon_x}$	38 ± 1	-2 ± 1
	$\frac{\partial Q_x}{\partial \epsilon_y} = \frac{\partial Q_y}{\partial \epsilon_x}$	1 ± 1	-3 ± 2
	$\frac{\partial Q_y}{\partial \epsilon_y}$	-44 ± 1	2 ± 1

was still possible to obtain a good measurement of amplitude detuning. Table 3 details the amplitude detuning coefficients obtained for the two cases.

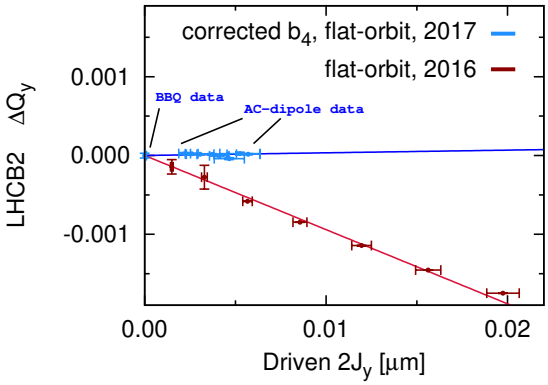

Fig. 13: Example of amplitude detuning measurements at $\beta^* = 0.3\,\mathrm{m}$ after IR-octupole correction (blue), and $\beta^* = 0.4\,\mathrm{m}$ before correction (red).

Application of normal octupole corrections in the ATLAS and CMS insertions substantially reduced the direct detuning terms, with minimal disruption to the already small cross-term detuning. One detuning term for Beam 1 ($\frac{\partial Q_y}{\partial \epsilon_y}$) could not be measured after correction, however as both errors and correctors are common to the two beams it may be confidently constrained to the same level as the measured detuning coefficients after correction. The observed reduction in amplitude detuning provides a direct validation of the global quality of the b_4 correction, and achieves one of the main aims of the nonlinear optics commissioning: removing the IR-contribution to the tune-spread in the squeeze. The small level of residual detuning and the stability of the correction/errors was also re-validated over larger amplitude ranges in late 2017 [63] and early 2018 [59].

The local nature of the normal octupole correction can also be confirmed by examining feed-down to tune as a function of crossing-angle. Figure 14 compares the Q_y dependence on the vertical crossing angle in IP1 measured in 2015, to that observed after b_4 correction in 2017. Application of the normal octupole correction has resulted in a substantially more linear tune shift as a function of the applied closed-orbit distortion in the IR. Reductions to the quadratic variation of tune with crossing-angle were observed in both IPs.

Direct RDT measurement was not used in calculation of the correction. Using the techniques

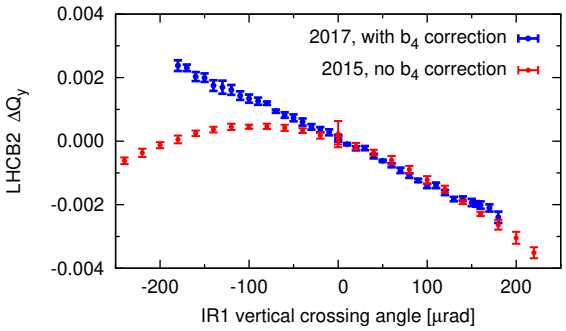

Fig. 14: Tune shift with crossing angle with (blue) and without (red) correction of normal octupole errors.

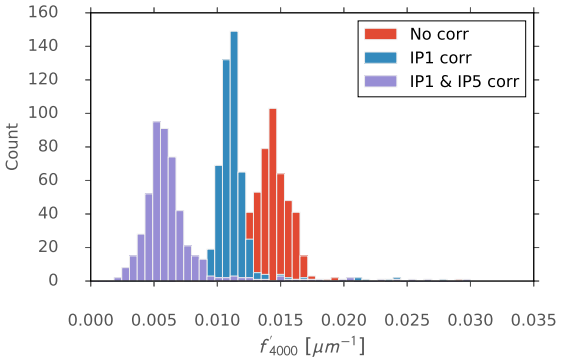

Fig. 15: Histogram of the f'_{4000} AC-dipole resonance driving term, related to the $4Q_x$ resonance, measured in LHC BPMs with and without correction of normal octupole errors in the ATLAS and CMS insertions.

developed in [52, 56] however, some AC-dipole RDTs could be observed, which provided further validation of the normal octupole correction. In particular, correction of normal octupole errors in both IR1 and IR5 significantly reduced the strength of the $4Q_x$ resonance. This is seen in Fig. 15, which shows histograms of the f'_{4000} resonance driving term measured in the LHC BPMs (where f' indicates a RDT for driven motion with an AC-dipole [55]) with and without correction of the normal octupole errors in the ATLAS and CMS insertions.

Application of the IR-b_4 correction was also found to substantially increase beam-lifetime in machine studies to test the β^* reach of the LHC. At $\beta^* = 0.14\,\mathrm{m}$, it was found that lifetime was so low as to inhibit linear optics measurement and correction. In response the IR-b_4 correction was applied. Figure 16 shows the change in fractional intensity recorded for the two minutes before (red) and after (blue) application of the normal octupole correction.

3.2 Normal sextupole correction in the CMS insertion

Due to the horizontal orientation of the crossing-angle plane in the CMS experimental insertion (IR5), normal sextupole errors feed-down to generate a normal quadrupole (b_2) perturbation. The errors may be examined by considering the linear variation of tune-shift with the horizontal crossing angle in IR5. Figure 17 (red) shows the measured tune-shift as a function of the applied crossing-angle bump for LHC Beam 1. A large asymmetry is observed between the linear variation of Q_x and Q_y with crossing angle, with sextupolar feed-down mainly perturbing the horizontal plane of Beam 1. Similar results were obtained for Beam 2, with feed-down mainly influencing the vertical plane. Some residual quadratic variation of tune with crossing angle can also be observed to remain after b_4 correction.

In order to compensate for the normal sextupole errors, linear variation of tune with crossing-angle

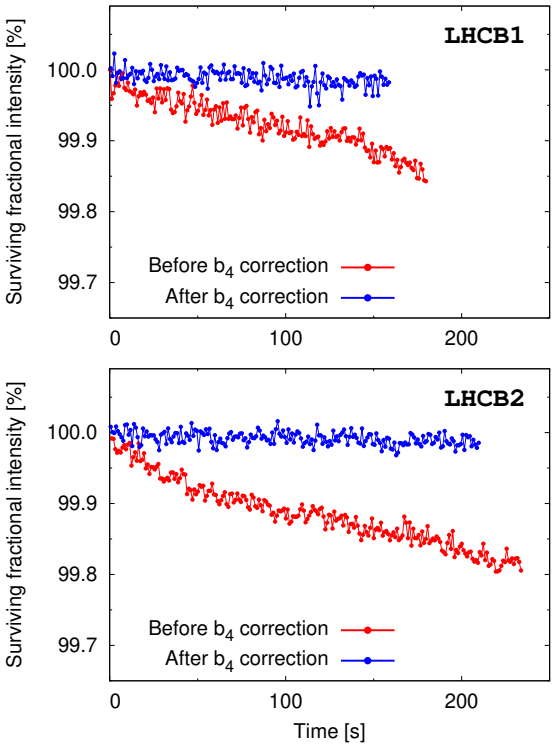

Fig. 16: Change in fractional intensity determined from Beam-Current Transformer data, for the two minutes prior (red), and following (blue), application of IR-b_4 corrections in IR1 and IR5. Measurements performed at $\beta^* = 0.14\,\mathrm{m}$ during dedicated tests of the ATS optics [64, 65].

(determined from second-order polynomial fits) was matched in MAD-X, using the b_3 corrector circuits left and right of IR5. The matching was performed simultaneously for Beam 1 and Beam 2. Settings of these common correctors, which reproduced the linear tune shift of both beams, were reversed and applied in the accelerator. Blue data in Fig. 17 shows the result of a crossing-angle scan performed after correction. The gray line shows the expected variation of tune if the predicted impact of the correction on linear tune-shift is applied to the pre-correction fits. The linear component of the tune shift was substantially reduced, and the observed variation after correction agrees well with expectation. Figure 18 compares the applied beam-based correction to the expectation from magnetic measurements. A discrepancy exists between beam- and magnetic-measurements. This is not unexpected given the preliminary studies performed in Run 1. The discrepancy remains to be understood, however it was also observed in Run 1 that missalignments of the normal octupole correctors, for example, could generate additional feed-down capable of influencing the lower order corrections [48]. Such effects may offer a potential explanation, but would require additional measurements to confirm.

During luminosity production the LHC operates very close to the linear coupling ($Q_{x,frac} - Q_{y,frac} = 0$) resonance, with fractional tune separation in the range $\Delta Q_{\mathrm{frac}} = 0.01 - 0.004$. Table 4 details the changes to fractional tune separation expected during crossing-angle levelling due to feed-down in IR5. Prior to normal sextupole correction, reduction of the IR5 crossing-angle from 150 to $100\,\mu\mathrm{rad}$ during luminosity levelling would give a $\sim 30\,\%$ reduction to the tune separation at $\beta^* = 0.4\,\mathrm{m}$ (reaching $\sim 40\,\%$ at $\beta^* = 0.3\,\mathrm{m}$). Application of the normal sextupole correction therefore represents a very significant improvement to tune stability during luminosity production. This is critical to maintaining Landau damping (which is dependent on linear coupling in relation to tune separation [31, 32]) as well as being potentially significant for beam-lifetime (tune shifts due to feed-down from IR-nonlinear errors can generate transient beam-losses [65] as well as shift the working point to sub-optimal regions

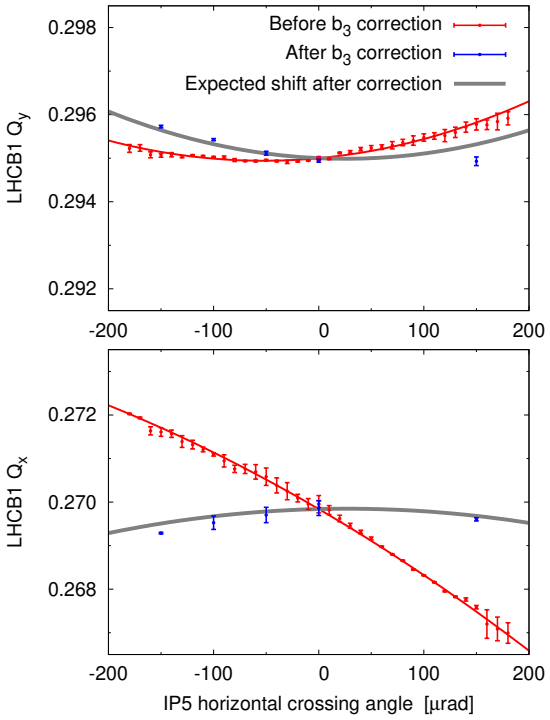

Fig. 17: Tune shift of LHC Beam 1 as a function of the horizontal crossing-angle in IR5. Red data show the tune shift measured after application of b_4 corrections, but before correction of b_3. The fit to the measured data is also shown in red. Blue data corresponds to the tune shift measured after application of b_3 corrections. The gray line indicates the expected variation of tune after b_3 correction, based upon the fit to red data and the expected performance of the b_3 correction.

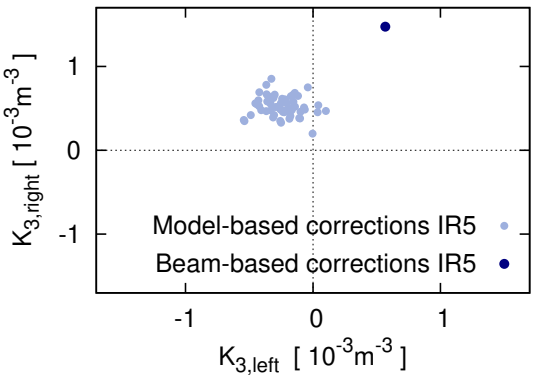

Fig. 18: Beam-based corrections for the normal sextupole errors applied in the CMS insertion, compared to the expected corrections based upon magnetic measurements. Sixty instances of the model-based corrections are shown, corresponding to the uncertainty in the magnetic measurements.

Table 4: Change to tune separation during LHC crossing-angle levelling, due to feed-down in the CMS insertion before and after correction of normal sextupole errors. Values quoted assume that linear coupling is small in relation to the tune separation. Values in [%] are quoted relative to the minimum tune separation used during luminosity production in 2017.

	Before corr $[10^{-3}]$	After corr $[10^{-3}]$
LHCB1 $\Delta\lvert Q_{x,\mathrm{frac}} - Q_{y,\mathrm{frac}}\rvert$	-1.22 ± 0.01	-0.32 ± 0.02
LHCB1 $\frac{\Delta\lvert Q_{x,\mathrm{frac}} - Q_{y,\mathrm{frac}}\rvert}{\lvert Q_{x,\mathrm{frac}} - Q_{y,\mathrm{frac}}\rvert}$	$-30\,\%$	$-7\,\%$
LHCB2 $\Delta\lvert Q_{x,\mathrm{frac}} - Q_{y,\mathrm{frac}}\rvert$	-0.80 ± 0.01	-0.44 ± 0.01
LHCB2 $\frac{\Delta\lvert Q_{x,\mathrm{frac}} - Q_{y,\mathrm{frac}}\rvert}{\lvert Q_{x,\mathrm{frac}} - Q_{y,\mathrm{frac}}\rvert}$	$-20\,\%$	$-10\,\%$

of the tune diagram).

While reduction of tune shift with crossing angle is of operational benefit, the main concern in relation to b_3 errors in the IRs is perturbation of linear optics. Figure 19 shows histograms of the change in beta-beating at $\beta^* = 0.4\,\mathrm{m}$ between $\pm 150\,\mu\mathrm{rad}$ crossing-angles, as measured in the BPMs around the LHC ring. This differential beta-beat due to sextupolar feed-down (before correction, red) is non-negligible in relation to the LHC's stated aim of achieving a $1\,\%$ tolerance on the beta-beating [7], and will increase for smaller β^*. This contribution had never previously been considered. The optics quality obtained during previous years' commissioning with flat closed-orbit [6, 7] thus represents a slight underestimate of the true β-beat during operation for luminosity production, where crossing-angles are applied. After minimization of linear tune variation with crossing-angle using the b_3 correctors in IR5, Fig. 19 (blue) shows a pronounced improvement to the distribution of the differential beta-beat vs crossing-angle measured in the LHC BPMs. Beta-beating in the vertical plane of Beam 1 and horizontal plane of Beam 2 was relatively stable before correction (comparable to Fig. 19 after correction), and was unaffected by the sextupole trims.

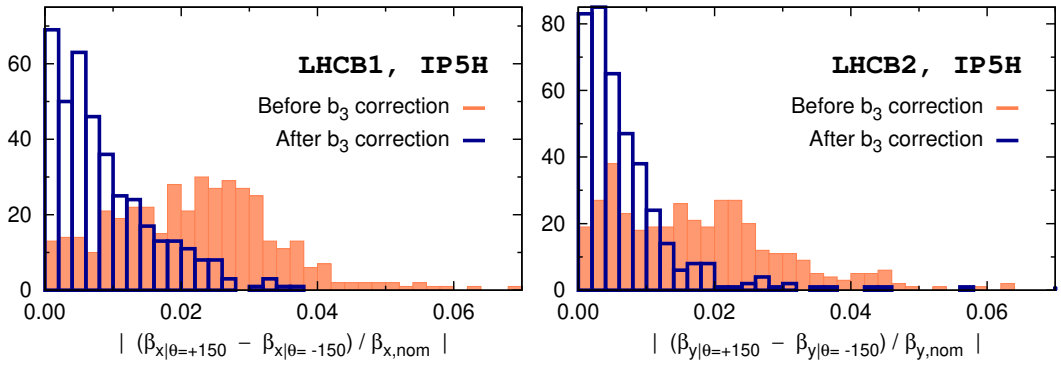

Fig. 19: Histograms of Beam 1 (top) and Beam 2 (bottom) beta-beating measured at LHC BPMs, before (blue) and after (red) normal sextupole compensation in IR5.

3.3 Normal sextupole, skew sextupole, and skew octupole correction in the ATLAS insertion

In contrast to the CMS insertion, the crossing plane for the ATLAS experiment is orientated vertically. In IP1 therefore normal sextupole errors feed-down to generate linear coupling as a function of the applied crossing angle. Skew octupole errors feed-down both horizontally and vertically to generate linear coupling. In IR5 linear coupling shifts going from 0 to $150\,\mu\mathrm{rad}$ (the operational crossing-angle

Table 5: Beam- and model- based corrections for skew octupole errors in IR1. Note that the a_4 corrector right of IR1 is broken and is not considered in the beam-based correction.

	Beam-based	Model-based
a_4 left IR1 $[\mathrm{m}^{-4}]$	$-$	$+0.81 \pm 0.04$
a_4 right IR1 $[\mathrm{m}^{-4}]$	$+1.0$	$+0.12 \pm 0.05$

Table 6: Strength of the f'_{1210} skew-octupole RDT before and after application of correction for a_4 feed-down. Values are the average absolute resonance strength measured around the ring.

	$\langle \lvert f'_{1210} \rvert \rangle$ $[\mu\mathrm{m}^{-1}]$	
	Beam 1	Beam 2
Before correction	0.37 ± 0.02	0.51 ± 0.02
After correction	0.45 ± 0.02	0.35 ± 0.01

for IR1 and IR5 in 2017) were comparatively small. In the ATLAS insertion however, large coupling shifts were seen in LHC Beam 2, motivating correction of both normal sextupoles and skew octupoles in this IR.

Figure 20 shows the real and imaginary parts of the f_{1001} RDT, driving the $(Q_x - Q_y)$ coupling resonance, as a function of the crossing-angle in IR1. Values have been multiplied by $4|Q_{x,\mathrm{frac}} - Q_{y,\mathrm{frac}}|$ to give the RDT in equivalent units to the linear coupling [39, 41]. Before correction (red) significant linear and quadratic variations of the coupling RDT can be observed, corresponding to feed-down from normal sextupole and skew octupole errors respectively. While normal sextupole correctors were available on both sides of IP1, the skew octupole corrector left of the IR is broken in the LHC. Settings of the three available correctors to minimize the linear and quadratic variation of coupling with crossing angle were found in MAD-X and applied to the machine. Blue data in Fig. 20 show the coupling measured after application of the correction, which has resulted in a substantial reduction in feed-down to coupling.

Coupling data obtained for Beam 1 before correction were low quality (Fig. 21) and only used to provide a constraint on the maximum allowed coupling shift generated by the normal sextupole and skew octupole trims. After correction, the coupling shift versus crossing-angle was comparable to Beam 2.

Table 5 details the applied skew octupole correction in IR1, together with the expected corrections based upon magnetic measurements. Due to the broken a_4 corrector on the left side of IR1 the beam- and model- based corrections cannot be compared directly. Recalling from Eq. (1) however, that for even-order multipoles contributions from the left and right sides of the IR add for the same sign of K_n, the beam-based correction found in 2017 suggests the total skew octupole contribution from the ATLAS insertion is comparable to that expected from the magnetic model.

Since linear coupling depends on $\sqrt{\beta_x \beta_y} e^{i[\phi_x - \phi_y]}$ which does not differ significantly between nonlinear correctors on the left and right sides of the IR, correction of skew-octupolar feed-down to coupling is still viable using a single corrector. Direct correction of the skew-octupole however, requires two functioning correctors [46]. Consequently the beam-based skew-octupole correction for IR1 coupling feed-down cannot represent an optimal correction of a_4 resonances. It was found that the coupling-based correction reduced the strength of the f'_{1210} RDT driving the $Q_x - Q_y$ resonance in Beam 2 while increasing the (initially smaller) RDT of Beam 1. Details of the RDT values before and after correction are given in Tab. 6. Given the emerging importance of skew-octupole sources directly to footprint distortion (and hence instabilities) in the LHC [30, 66] alternative strategies based upon RDT compensation using the three available correctors in IR1 and IR5 are also being pursued [52, 56].

Considering Fig. 20, the normal sextupole correction applied in 2017 overcompensated the linear

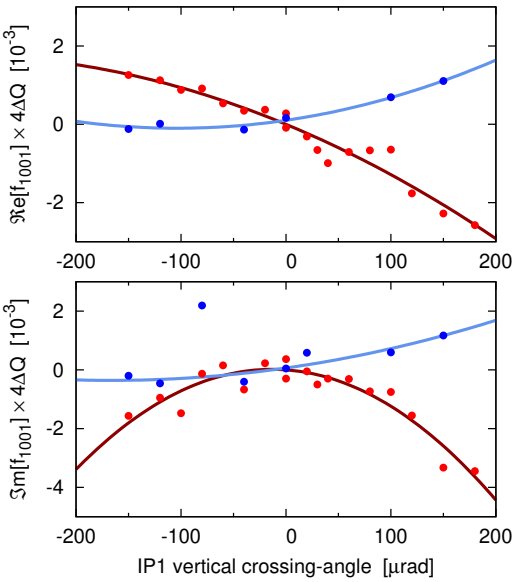

Fig. 20: Change to real and imaginary parts of the Beam 2 linear coupling RDT f_{1001}, as a function of vertical crossing angle in the ATLAS insertion. Measurements before normal sextupole and skew octupole correction are shown in red, after correction in blue. The coupling is expressed in units equivalent to $|C^-|$.

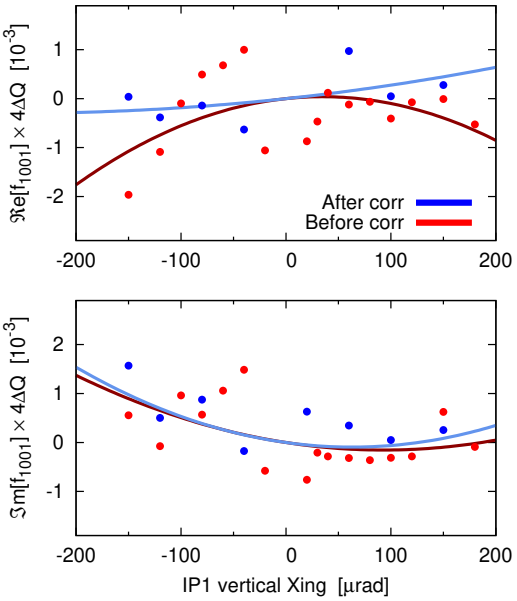

Fig. 21: Change to real and imaginary parts of the Beam 1 linear coupling RDT f_{1001}, as a function of vertical crossing angle in the ATLAS insertion. Measurements before normal sextupole and skew octupole correction are shown in red, after correction in blue. The coupling is expressed in units equivalent to $|C^-|$.

coupling shift with IR1 vertical crossing-angle. Additionally correction based only on feed-down to linear coupling gives a relatively weak constraint on how the correction should be balanced between the left and right sides of the IR. The β-dependence of linear coupling RDTs evaluated at the correctors gives

$$\sqrt{\beta_x\beta_y}|_{\text{left corrector}} \approx \sqrt{\beta_x\beta_y}|_{\text{right corrector}}$$

Together with the $\sim \pi$ phase advances between the left and right sides of the IR, this means that either corrector can generate a similar behaviour to that located on the other side of the IR. Constraint on the correction mainly comes therefore from the different orbit offsets of the two beams at each corrector. As previously mentioned however, the Beam 1 coupling measurements obtained during 2017 commissioning were of low quality. The normal sextupole correction was thus relatively weakly constrained in 2017. This prompted a re-visit of the normal sextupole correction in 2018.

While feed-down to linear coupling as a function of the vertical crossing-angle is the observable of operational relevance for normal sextupole errors in IR1, it is not the only observable which can be used to determine sextupole corrections. While operationally irrelevant, a horizontal (as opposed to vertical) crossing-angle bump was used to generate feed-down from the normal sextupole errors to tune (as opposed to linear coupling). The different $\beta_{x,y}$-dependence of feed-down to Q_x and Q_y provides additional constraints on the left/right balance of the normal sextupole correction. Thus in 2018, settings of the b_3 correctors either side of the ATLAS insertion were powered in order to minimize for both beams the linear change of the $\Re e$ and $\Im m$ coupling as a function of vertical crossing-angle, and also to minimize the linear change of $Q_{x,y}$ as a function of the horizontal crossing-angle. Coupling measurement quality was also improved by moving the working point closer to the relevant coupling resonance to enhance the f_{1001} RDT being measured. This evolution to the correction procedure resulted in a significant change to the sextupole settings between 2017 and 2018, as seen in Fig. 22.

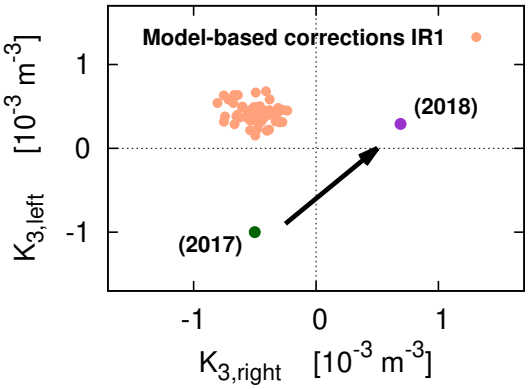

Fig. 22: Beam- and model-based correction (2017 and 2018) for normal sextupole errors in the ATLAS IR, compared to the expected corrections based upon magnetic measurements.

The improvement to variation of coupling as a function of the vertical crossing-angle in 2018 was clear, but modest when compared to the significant reduction to $\Re e[f_{1001}]$ of Beam 2 in 2017. Figure 23 shows an example of the improved feed-down to coupling, while Tab. 7 gives details of the linear variation of coupling with the various configurations of the normal sextupole correctors.

The exact $|C^-|$ generated by feed-down from the sextupole and octupole errors in IR1 is dependent on the initial phase of the f_{1001} resonance driving term, and how the real and imaginary components of the RDT are enhanced or cancelled by feed-down. In the most extreme case (both $\Re e$ and $\Im m$ add) feed-down from the experimental insertion is capable of generating substantial linear coupling via changes of crossing-angle during luminosity levelling. Table 8 details the coupling shifts which could be generated during crossing-angle levelling from $150\,\mu\text{rad} \rightarrow 100\,\mu\text{rad}$ before and after correction of normal-sextupole and skew-octupole errors in IR1.

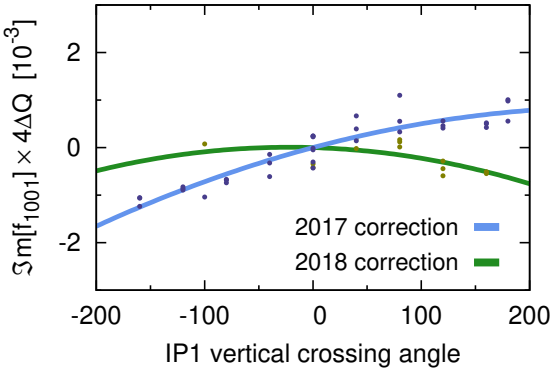

Fig. 23: Change to the imaginary part of the f_{1001} coupling RDT as a function of vertical crossing angle in IR1, before and after iteration of the normal sextupole correction in 2018.

Table 7: Linear variation of coupling RDT with vertical crossing angle in IR1 at $\beta^* = 0.4\,\mathrm{m}$, from a quadratic fit.

Beam 1	$\frac{\partial}{\partial\theta}\Re e\,[f_{1001}] \times 4\Delta Q$ $[10^{-6}]$	$\frac{\partial}{\partial\theta}\Im m\,[f_{1001}] \times 4\Delta Q$ $[10^{-6}]$
No correction	–	–
2017 correction	6.7 ± 0.4	1.4 ± 0.7
2018 correction	3.3 ± 1.3	0.0 ± 1.1
Beam 2	$\frac{\partial}{\partial\theta}\Re e\,[f_{1001}] \times 4\Delta Q$ $[10^{-6}]$	$\frac{\partial}{\partial\theta}\Im m\,[f_{1001}] \times 4\Delta Q$ $[10^{-6}]$
No correction	-10.1 ± 0.7	-2.6 ± 1.1
2017 correction	2.1 ± 0.3	6.1 ± 0.4
2018 correction	-0.1 ± 0.5	-0.7 ± 1.3

Table 8: Maximum possible changes in linear coupling which can be generated due to normal sextupole and skew octupole feed-down from the IR1 insertion during crossing-angle levelling of LHC luminosity. Values for $\beta^* = 0.3\,\mathrm{m}$ are based on the expected scaling of the feed-down with β^*.

	$\Delta\lvert C^-\rvert\ [10^{-3}]$		$\frac{\Delta\lvert C^-\rvert}{Q_{x,\mathrm{frac}}-Q_{y,\mathrm{frac}}}$
	$\beta^* = 0.4\,\mathrm{m}$	$\beta^* = 0.3\,\mathrm{m}$	$\beta^* = 0.3\,\mathrm{m}$
No correction	≤ 1.5	≤ 2.0	$\leq 50\,\%$
After correction	≤ 0.4	≤ 0.6	$\leq 15\,\%$

Before correction of normal-sextupole and skew-octupole nonlinearities in the ATLAS insertion, luminosity levelling at $\beta^* = 0.3\,\mathrm{m}$ could generate coupling up to $\sim 1/2$ of the minimal fractional tune separation used during luminosity production. A $|C^-|$ of $\frac{1}{2}$ the tune separation is known to be incompatible with successful LHC operation, and even at the larger tune separation an additional $\Delta|C^-| = 0.002$ can risk loss of Landau damping if the initial coupling is poorly corrected ($|C^-|_{\mathrm{initial}} > 0.002$) [32]. Correction of normal-sextupole and skew-octupole errors, beginning in 2017 and continuing into 2018 operation, therefore represents a significant operational improvement, which plays a valuable role in facilitating the introduction of crossing-angle luminosity levelling into regular LHC operation since 2017.

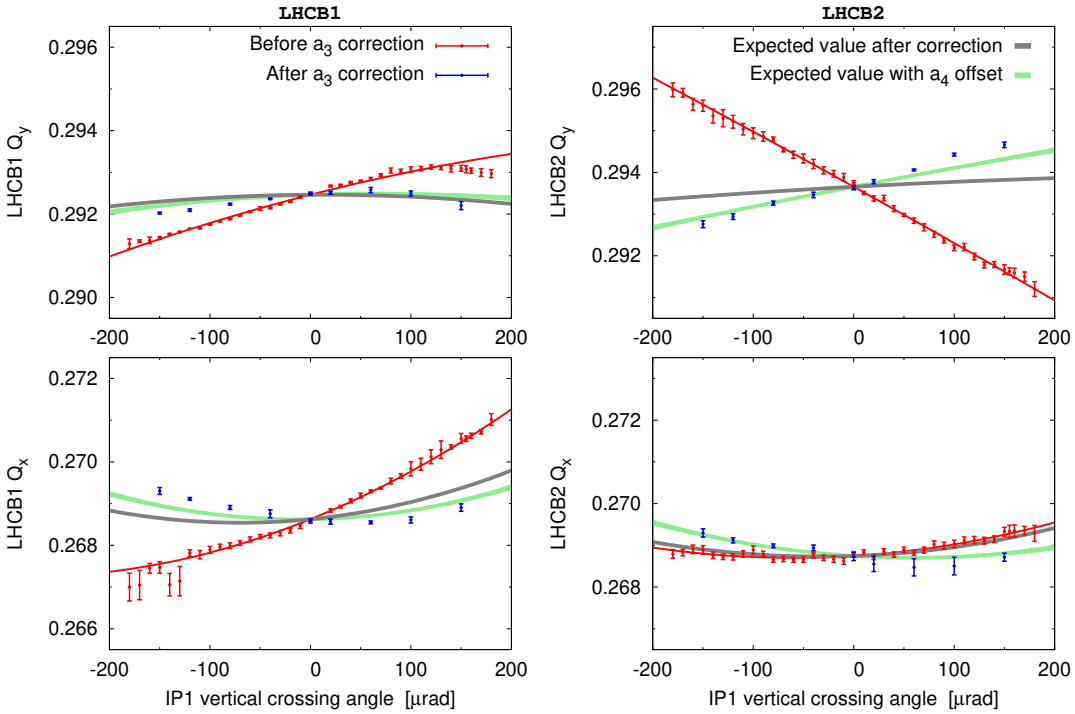

Fig. 24: Tune shift of LHC Beam 1 (left) and LHC Beam 2 (right) as a function of vertical crossing-angle in IR1. Red data shows the tune shift measured after application of b_4 corrections, but before correction of a_3, b_3 or a_4. The fit to the measured data is also shown in red. Blue data corresponds to the tune shift measured after application of a_3, b_3, and a_4 corrections. The gray line indicates the expected variation of tune after correction, based upon the red fit and expected performance of the a_3 correction. The green line represents the expected variation after correction, where the measured Q-shift during application of the skew octupole correction has been incorporated as a source of linear tune variation.

In parallel with compensation of feed-down to linear coupling, skew sextupoles in IR1 (which feed-down via the vertical IR1 crossing angle to generate normal quadrupole perturbations) were also compensated. Echoing normal sextupole correction in IR5, skew sextupole correction in IR1 was performed via minimization of the linear part of the tune shift as a function of the vertical crossing angle in IR1. Figure 24 shows the feed-down to tune of LHC Beam 1 (left) and Beam 2 (right) before correction (red) and after correction (blue). The expected tune variation after correction is also shown in gray.

A significant improvement to tune-shift vs crossing angle was obtained via application of the skew sextupole correction, however a clear discrepancy can be observed between the expected (gray) and obtained (blue) tune variation after correction. The discrepancy appeared for both planes of both LHC beams, and was not the result of tune drift. The difference between expected and obtained behaviour was the consequence of the application of the skew-sextupole correction for tune feed-down in parallel with with skew-octupole correction for feed-down to coupling. Pre-correction measurements (red) were performed with only the normal octupole corrections described in Sec. 3.1 applied. Post-correction measurements (blue) were performed with corrections for skew sextupole, normal sextupole and skew octupole applied. Skew octupoles feed-down to linear coupling, with a quadratic dependence on both the horizontal and vertical offset of the beam through the a_4 source ($\propto \Delta x^2 + \Delta y^2$). In the case of purely horizontal or vertical offset therefore, the skew-octupole correction should not influence the LHC tune. In the case of a diagonal offset of the beam through the a_4 source however ($\propto \Delta x \Delta y$) a skew octupole also generates feed-down to tune. Thus, for example, a horizontal misalignment of the a_4 corrector in IR1 would generate an additional source of linear tune variation as a function of the vertical crossing angle. Figure 25 shows the vertical tune as a function of time, while the skew octupole correction is

turned on, for a vertical crossing angle of $150\,\mu\mathrm{rad}$ in IR1. A clear shift to tune was observed to $Q_{x,y}$ of both beams. Application of the a_4 correction in Fig. 25 was performed with a large tune separation ($\Delta Q_{x,y} = 0.028$), thus even though a significant coupling shift was generated (Fig. 20) the impact of this coupling shift on the tune is significantly smaller than observed in Fig. 25 (using [67]). Assuming therefore, that the tune-shifts measured during application of the a_4 correction are dominated by feed-down due to a constant horizontal offset of the beams through the a_4 corrector in conjunction with the applied $150\,\mu\mathrm{rad}$ vertical crossing-angle, the expected linear variation of tune as a function of vertical crossing angle after correction of a_3 is modified, as shown by the green lines in Fig. 24, which are comparable to the measured change of tune observed with skew sextupole and skew octupole corrections applied.

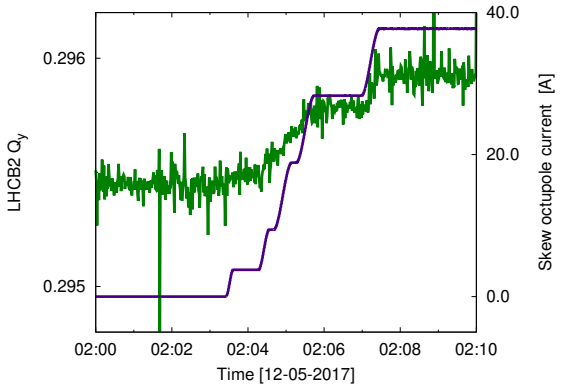

Fig. 25: Change to Q_y of Beam 2 upon application of skew-octupole correction for feed-down to $|C^-|$, with a $150\,\mu\mathrm{rad}$ vertical crossing angle in IR1.

Simulations in MAD-X were used to examine the transverse offset of the a_4 corrector required to explain the observed tune shifts during application of the a_4 correction (as seen in Fig. 25) and the discrepancy between the expected (gray) and observed (blue) linear variation of tune with IR1 vertical crossing-angle (as seen in Fig. 24). A $1\,\mathrm{mm}$ horizontal misalignment of the skew octupole corrector towards the outside of the ring could explain the observed discrepancy for both LHC Beams (equivalently this could also correspond to a closed-orbit error of both beams towards the inside of the ring). An alternative explanation is that cross-talk of the a_4 corrector with the skew-sextupole (skew sextupole and octupole corrector magnets are nested in the same assembly) can modify the transfer function of the a_3 corrector. In either case the additional linear tune variation generated by feed-down or cross-talk of the skew octupole can be corrected via an iteration of the skew sextupole correction on the right side of IP1. Such an iteration was not performed during commissioning of the $\beta^* = 0.4\,\mathrm{m}$ optics in 2017, but has since been applied to optics used for operation at $\beta^* < 0.4\,\mathrm{m}$ in 2017 and 2018. Figure 26 shows the beam-based skew sextupole corrections before and after this iteration. The observation that feed-down and/or cross-talk from a higher-order correction spoiled sextupole compensation is significant for future LHC commissioning, and demonstrates the need for iterative compensation between multipole orders.

A slight improvement to linear optics stability versus crossing-angle was observed upon application of the skew sextupole correction in IR1, though less pronounced than that obtained via normal sextupole correction in IR5 (possibly also a consequence of additional beta-beat generated by feed-down from the skew octupole correction). Figure 27 shows the distribution of the relative change in β measured around the LHC ring in the horizontal plane of Beam 1 and Vertical plane of Beam 2. Slight improvements can be discerned, particularly for Beam 2. The vertical plane of Beam 1 and horizontal plane of Beam 2 showed no noticeable change to the distribution of differential beta-beat.

While only a limited improvement to the linear optics was observed upon skew sextupole compensation, the applied corrections were clearly beneficial to compensation of the main skew sextupole reso-

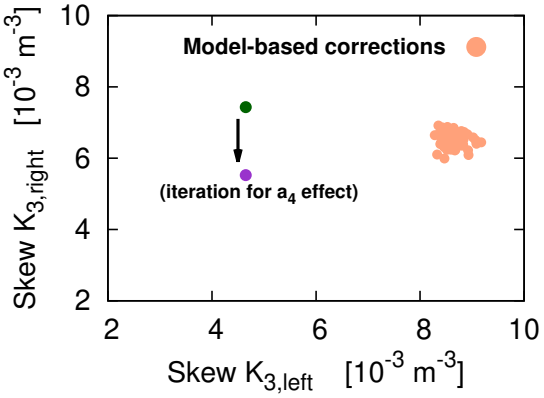

Fig. 26: Beam- and model-based correction of skew sextupole errors in the ATLAS insertion.

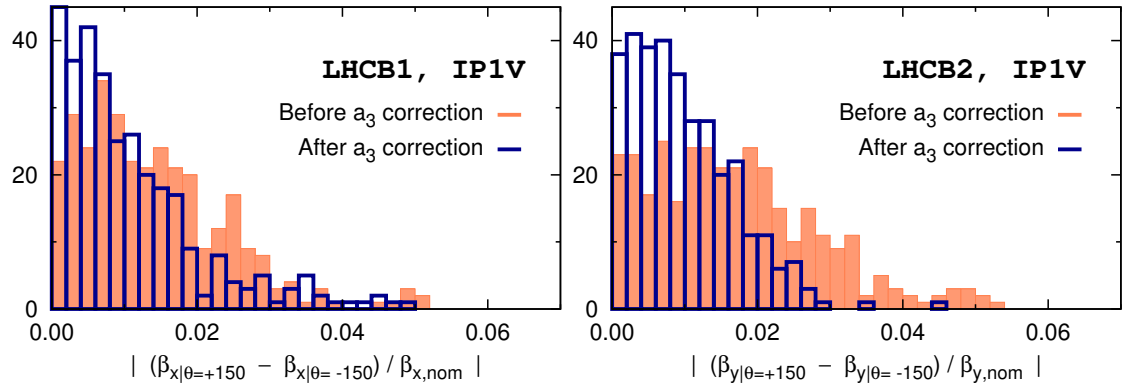

Fig. 27: Histograms of beta-beating measured at LHC BPMs, before (blue) and after (red) skew sextupole compensation in IR1.

nance of operational concern, specifically the $3Q_y$ resonance. Figure 28 shows histograms of the relevant f'_{0030} resonance driving term measured around the ring before and after skew sextupole compensation in IR1, using the methods developed in [52, 56] (where f' indicates an RDT for driven motion with an AC-dipole [55]). Once again RDTs were used not to calculate the IR-nonlinear corrections but to provide a validation of the correction calculated via feed-down. As with correction of normal sextupole errors in IR5 (Tab. 4) skew-sextupole compensation also significantly reduced the change to tune-separation and working-point anticipated during LHC luminosity levelling, which may actually represent the most significant operational benefit arising from the correction.

4 Linear re-optimization

Correction of normal sextupole errors in IR5 improved the stability of the linear optics as a function of the applied crossing scheme, as seen in Figs. 19. In spite of this improvement however, there remained a non-zero dependence of the beta-beat on crossing angle after the nonlinear corrections were applied. Figure 29 (top, center) compares the beta-beating measured in Beam 2 (with similar results obtained for Beam 1) after application of the nonlinear corrections and with the operational crossing-scheme applied, to that obtained after linear optics commissioning at flat-orbit as described in Sec. 2. A deterioration to the RMS beta-beat at the level of $\sim 1\,\%$ is observed. Figure 29 (bottom) also shows the significant normalized dispersion beating generated upon application of the crossing-scheme (note that in this case the dispersion beat is defined relative to models which include the corresponding settings of IR-orbit bumps as applied during the respective measurements). The LHC aims to achieve control of the optics at the $1\,\%$ RMS level [7]. The degradation of β-beat together with the clear deterioration of normalized

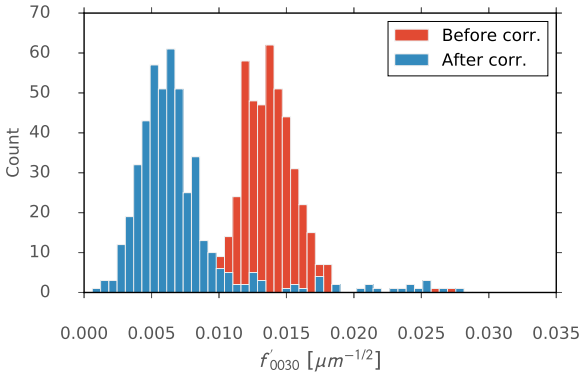

Fig. 28: Histogram of the f'_{0030} AC-dipole resonance driving term, related to the $3Q_y$ resonance, measured in LHC BPMs with and without correction of skew sextupole errors in the ATLAS insertion.

dispersion upon application of the crossing-scheme prompted a linear re-optimization of the optics in the operational configuration, using the global correction procedure outlined in Sec. 2. This is in contrast to previous years, where optics corrections were only performed at flat-orbit.

The method for optics measurements with the operational crossing-scheme based on AC-dipole excitation were unchanged from those described in Sec. 2, however K-modulation of the triplet quadrupoles resulted in the generation of significant closed-orbit distortions when attempted with the crossing-angles applied. This can be seen in Fig. 30, which shows clear modulation of the RMS orbit in the arcs (Fig. 30 bottom, green), as well as changes to the measured crossing-angle in IR1 (Fig. 30 center, red). K-modulation relies on precise measurement of tune-shifts generated by quadrupole modulation, requiring the tune shift to be measured at the level of $\Delta Q_{x,y} \leq 1 \times 10^{-5}$. The large orbit modulations present during measurement in the operational configuration risk distorting the β-measurement due to feed-down from nonlinear magnets and errors in the arcs, as well as any residual nonlinear errors remaining in the low-β IRs. Indeed, making a crude estimate based upon the observed $10\,\mu\mathrm{rad}$ modulation to crossing-angle observed in Fig. 30 together with the observed tune-shifts with crossing-angle seen in IR5 in Sec. 3.2 it is possible to anticipate an error on the tune modulation at the level of $\sim 2 \times 10^{-5}$ due only to the residual nonlinear errors remaining in a single IR. This estimate could rise to $\sim 6 \times 10^{-5}$ if the sextupole errors, for example, had not been corrected. These numbers should be taken to indicate a possible order-of-magnitude, and are not exact since orbit leakage generated during K-modulation is unlikely to give the exact same feed-down as the operational orbit-bumps, and the exact feed-down would depend on the contribution of many sources in the arcs and all IRs. To limit distortion of the tune modulation by feed-down from residual nonlinear errors in the IRs and from arc sextupoles, K-modulation was performed for the first time with an active orbit feed-back (OFB) operational during the measurement. As seen in Fig. 30 (yellow and green) application of the OFB significantly improved orbit leakage during the measurement, reducing the expected error on the tune modulation from the level of 10^{-5} to 10^{-6} after correction of IR-nonlinear errors. Table 9 gives an example of the effect application or removal of the orbit feed-back had on a β^* measurement performed during commissioning the operational configuration of the $\beta^* = 0.3\,\mathrm{m}$ optics in late 2017. Removal of the OFB introduces non-negligible distortions of the inferred β^* and waist values obtained via K-modulation, which would inhibit any attempt to correct the optics in the operational configuration.

Introduction of an orbit feed-back into K-modulation measurement in 2017 was essential to facilitate measurement of β^* with IR crossing-angle orbit bumps applied. This then allowed for the first correction of the linear optics in the true operational configuration of the LHC. An example of the linear re-optimization can be seen in Fig. 31 which compares the vertical β-beat of Beam 1 before and after application of the linear re-optimization in the operational configuration.

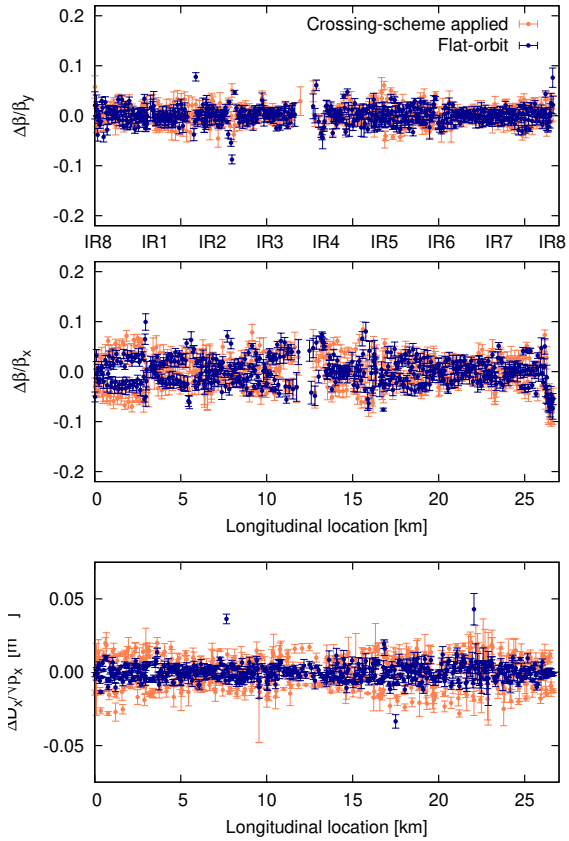

Fig. 29: Beta-beating (top,center) and normalized dispersion (bottom) of LHC Beam 2, measured at flat-orbit after application of global linear optics corrections, and at the operational crossing-scheme after application of all nonlinear corrections in 2017.

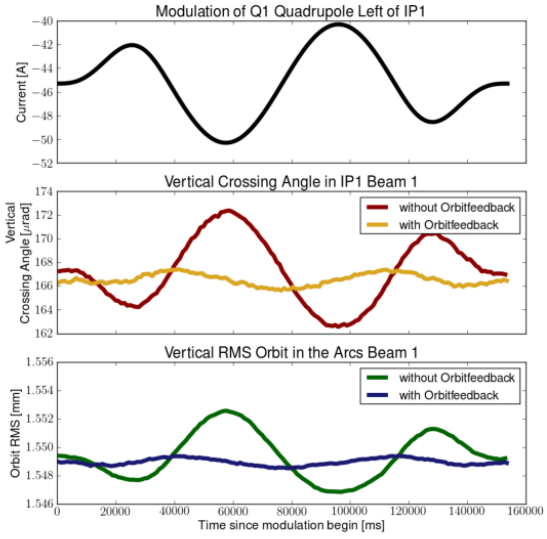

Fig. 30: Orbit leakage during K-modulation measurements performed in the operational configuration of the $\beta^* = 0.3\,\mathrm{m}$.

Table 9: Comparison of β^* and waist shift measurements performed via K-modulation, with and without any active orbit feed-back, during commissioning of the operational configuration of the $\beta^* = 0.3\,\mathrm{m}$.

Beam 1	with OFB	without OFB
β_x^* [m]	0.3018 ± 0.0007	0.2980 ± 0.0004
β_y^* [m]	0.3192 ± 0.0048	0.3064 ± 0.0027
β_x^* − Waist [m]	0.0234 ± 0.0039	0.0198 ± 0.0028
β_y^* − Waist [m]	-0.0837 ± 0.0081	-0.0606 ± 0.0062
Beam 2	with OFB	without OFB
β_x^* [m]	0.3107 ± 0.0014	0.3113 ± 0.0005
β_y^* [m]	0.2996 ± 0.0003	0.3064 ± 0.0011
β_x^* − Waist [m]	-0.0350 ± 0.0056	0.0173 ± 0.0040
β_y^* − Waist [m]	0.0072 ± 0.0043	0.0342 ± 0.0046

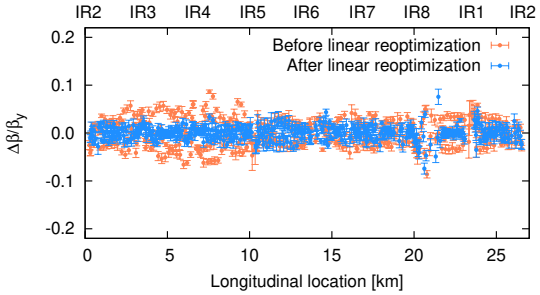

Fig. 31: Vertical β-beat of LHC Beam 1 before and after re-optimization of linear optics corrections at the operational configuration of the crossing-scheme.

Two iterations of linear corrections were performed for the operational crossing-scheme at $\beta^* = 0.4\,\mathrm{m}$, the latter aiming both to further reduce the global β-beat and improve the constraint on the phase advance between the dump kicker and triplet collimators (relevant to machine protection in the case of an uncontrolled firing). Table 10 summarizes the RMS β-beat and normalized dispersion obtained at various stages in the commissioning process, and compares the linear optics quality obtained for nominal LHC optics in 2016 with only flat-orbit. Going from 2017 commissioning with flat-orbit, to the operational crossing-scheme with nonlinear corrections applied, the most significant deterioration to $\Delta\beta/\beta$ can be observed in the vertical plane of Beam 1 and horizontal plane of Beam 2 (highlighted in red in Tab. 10) where there was a $\sim 1\,\%$ deterioration of the RMS β-beat. It should be noted that these are the values obtained after application of the normal sextupole correction in IR5 had already improved the stability of the linear optics as a function of crossing-angle. It is also worth noting that the largest deterioration to $\Delta\beta/\beta$ is observed in the two planes where the IR5 sextupole correction had a negligible impact (as discussed in Sec. 3.2). While such a deterioration is small, it is still relevant compared to the LHC's objective of $1\,\%$ optics control. Smaller increases to RMS β-beat were also observed in the other planes.

Application of linear optics corrections in the operational configuration was able to restore the RMS $\Delta\beta/\beta$ in the most severely affected planes to the same level present following 2017 commissioning at flat-orbit (highlighted in green in Tab. 10). The final β-beat obtained for ATS optics in the operational configuration at $0.4\,\mathrm{m}$ is also of comparable, but slightly worse, quality to that obtained for nominal optics at flat-orbit in 2016. In particular, the β-beat in the horizontal plane of both beams in 2017 is $\sim 1\,\%$

Table 10: Comparison of linear optics quality obtained with flat-orbit for the 2017 ATS optics at $0.4\,\mathrm{m}$, to that obtained with flat-orbit in 2016 for the nominal $0.4\,\mathrm{m}$ optics. Values for 2016 were taken from [7].

	2017 Flat-orbit (linear corrs)	2017 OP-crossing (after NL corrs)	2017 OP-crossing (after linear reoptimization)	2016 Flat-orbit (linear corrs)
Beam 1 $\beta_x\|_{\mathrm{RMS}}$ [%]	2.3	2.7	2.5	1.4
Beam 1 $\beta_y\|_{\mathrm{RMS}}$ [%]	1.5	2.8	1.3	1.8
Beam 2 $\beta_x\|_{\mathrm{RMS}}$ [%]	2.6	3.2	2.5	1.4
Beam 2 $\beta_y\|_{\mathrm{RMS}}$ [%]	1.5	1.8	1.8	1.4
Beam 1 $\frac{\Delta D_x}{\sqrt{\beta_x}}\|_{\mathrm{RMS}}$ $[10^{-2}\mathrm{m}^{-\frac{1}{2}}]$	0.45	0.96	0.73	0.52
Beam 2 $\frac{\Delta D_x}{\sqrt{\beta_x}}\|_{\mathrm{RMS}}$ $[10^{-2}\mathrm{m}^{-\frac{1}{2}}]$	0.58	1.11	0.61	0.62

worse than for 2016 (flat orbit). It can be seen from Tab. 10 however, that this pattern is also present at flat-orbit in 2017 and therefore appears to relate to either the transition to ATS optics or the decision not to iterate local-correction in 2017 (as described in Sec. 2) rather than any effect caused by considering the optics in the true operational configuration. Figures 32-34 show the final beta-beat obtained for the operational configuration of the LHC at $\beta^* = 0.4\,\mathrm{m}$, compared to the flat-orbit configuration measured in 2016.

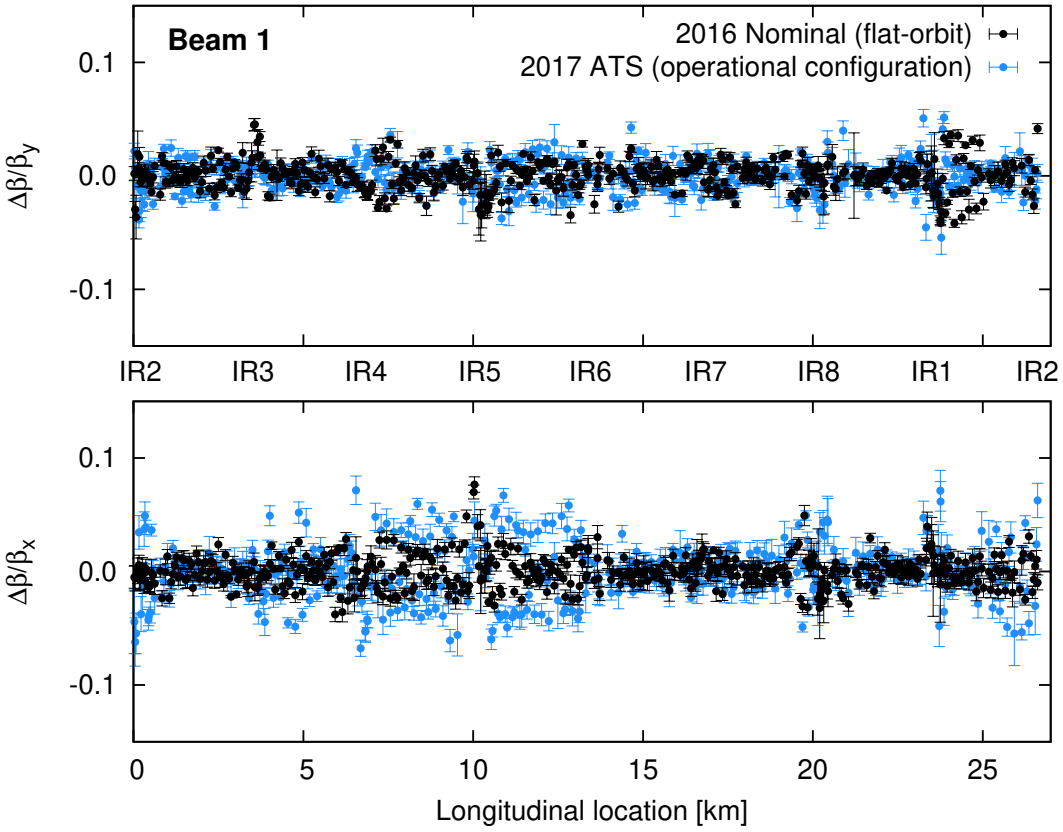

Fig. 32: β-beat in LHC Beam 1 measured for nominal optics in 2016 at flat-orbit and in 2017 for the operational configuration of ATS optics at $\beta^* = 0.4\,\mathrm{m}$.

As seen in Tab. 10, application of the crossing-angles approximately doubled the normalized dispersion beating (relative to models including the applied settings of the crossing-angles during measure-

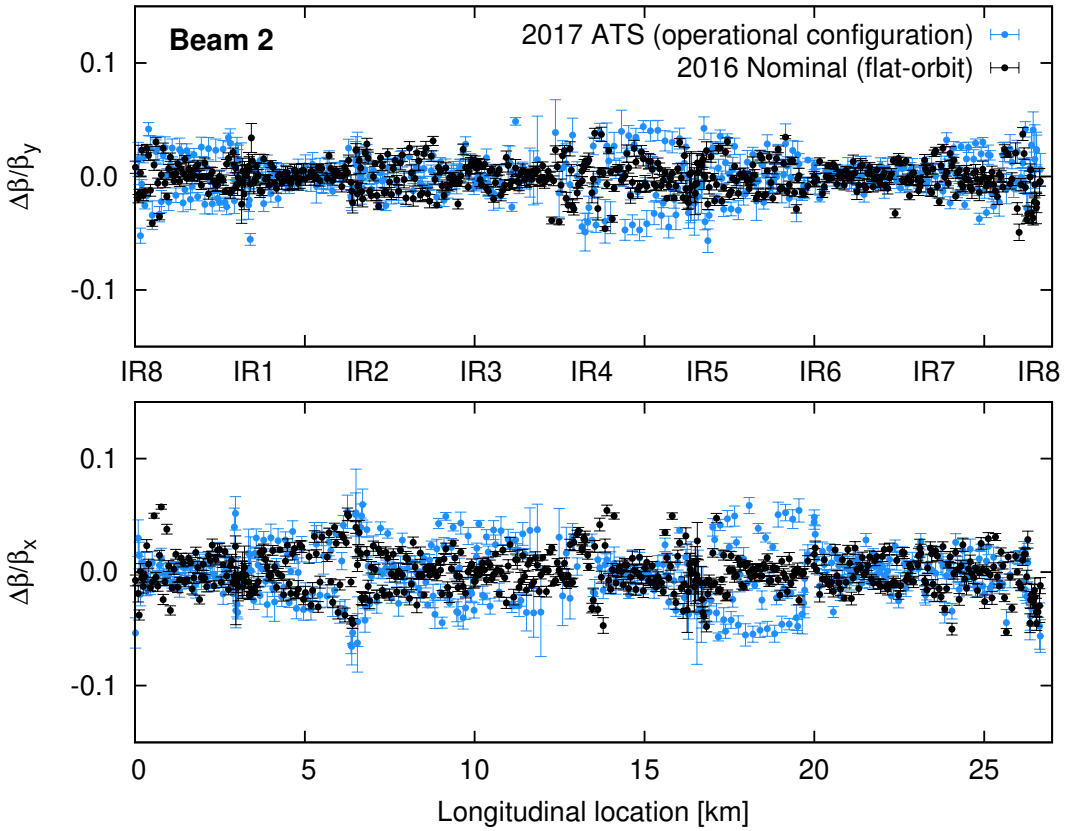

Fig. 33: β-beat in LHC Beam 2 measured for nominal optics in 2016 at flat-orbit and in 2017 for the operational configuration of ATS optics at $\beta^* = 0.4\,\mathrm{m}$.

ment). The re-iteration of the linear optics in the operational configuration efficiently reduced the dispersion beating of Beam 2 back to the level obtained for flat-orbit in 2016 and 2017. Figure 34 (bottom) compares the final normalized dispersion beat obtained for the operational configuration at $\beta^* = 0.4\,\mathrm{m}$ in 2017, to that obtained with a flat-orbit in 2016. The RMS $\Delta D_x/\sqrt{\beta_x}$ calculated for Beam 1 (highlighted in orange in Tab. 10) does not show such a clear reduction, however examining Fig. 34 (top, pale blue) the measurement quality for Beam 1 was particularly low, with typical BPM uncertainties larger than the calculated RMS making the calculated value unreliable compared to that obtained for Beam 2 and for 2016.

While control of beta-beat and normalized dispersion globally around the ring is of significant concern, the key parameter of relevance to luminosity production is β^*. Table 11 shows the β^* values measured via K-modulation in the ATLAS and CMS insertions for the operational configuration of the ATS crossing scheme in 2017, and compares them to the values obtained at flat-orbit for the nominal LHC optics in 2016. After re-optimization of the linear optics in 2017, the largest deviation from the desired β^* was $0.8 \pm 0.4\,\mathrm{cm}$ in the vertical plane of Beam 1 (highlighted in red in Tab. 11), which is comparable to the largest deviation obtained in 2016 ($0.5 \pm 0.1\,\mathrm{cm}$). This also represents a significant improvement compared to the $\sim 4\,\%$ β^*-beat obtained in this plane prior to the re-optimization of the linear optics. The Q_y measurement during K-modulation in this case suffered from significant noise, leading to larger uncertainty on the inferred β^*. Considering the K-modulation measurements more generally, re-optimization of the linear optics has systematically reduced β^* errors, to a level comparable to that obtained at flat-orbit in 2016. For all planes control of β^* was achieved at the level of $1-2\,\%$ for the operational configuration in 2017, a level which was previously only obtained for flat-orbit in previous years of LHC operation, and which would not have been obtained without further iteration of

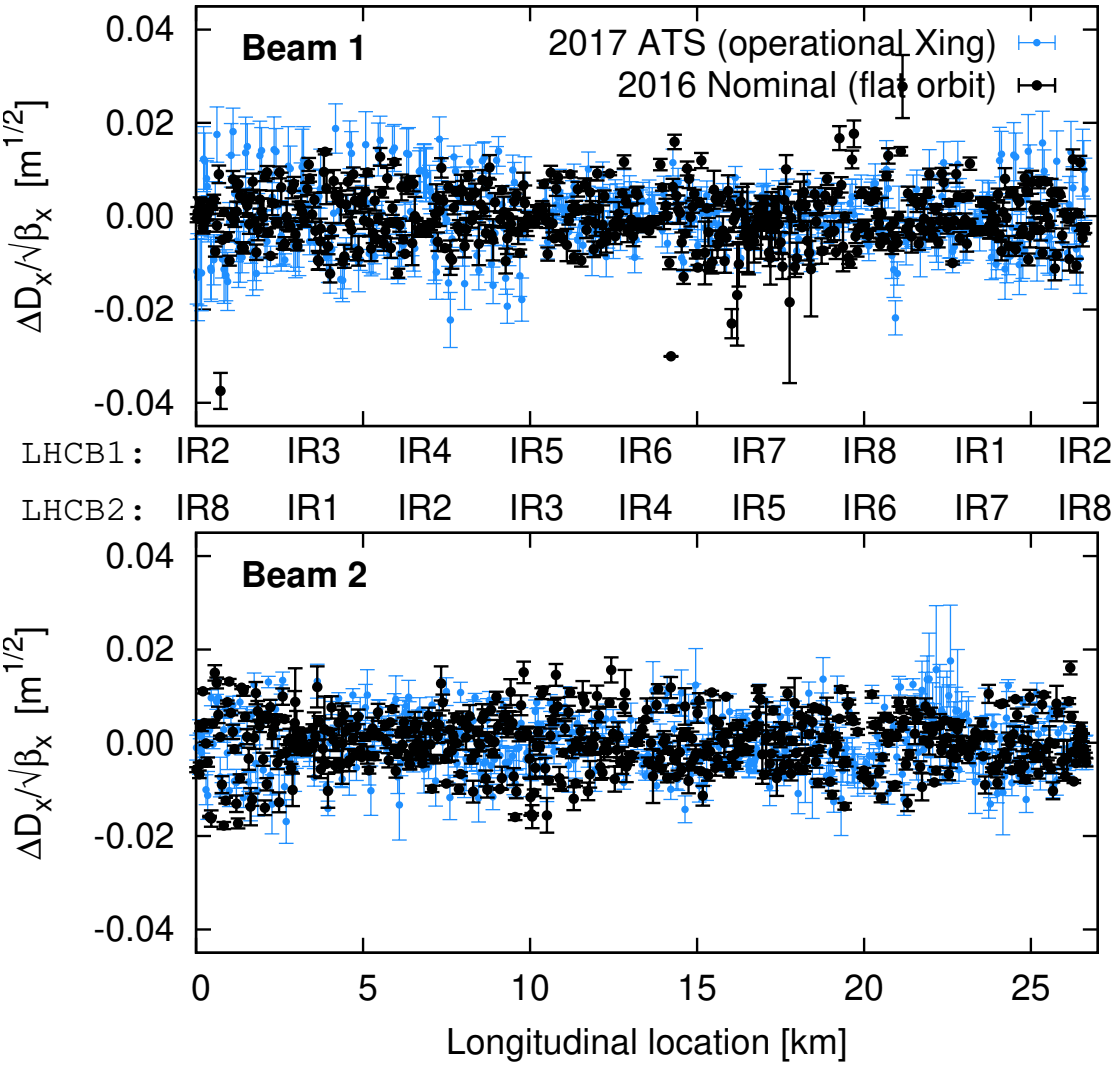

Fig. 34: Normalized dispersion at flat-orbit for LHC Beam 1 (top) and LHC Beam 2 (bottom), measured for nominal optics in 2016 at flat-orbit and in 2017 for the operational configuration of ATS optics at $\beta^* = 0.4\,\mathrm{m}$.

the optics corrections with the operational crossing-scheme applied.

The β^*-imbalance in Tab. 11 can be related to an expected luminosity imbalance between the ATLAS and CMS insertions. Prior to linear re-optimization of the optics the predicted lumiosity-imbalance due to β^* discrepancies would have been:

$$\frac{L_{\mathrm{CMS}}}{L_{\mathrm{ATLAS}}} = 0.974 \pm 0.004 \tag{4}$$

after linear re-optimization this value is significantly improved:

$$\frac{L_{\mathrm{CMS}}}{L_{\mathrm{ATLAS}}} = 1.003 \pm 0.004 \tag{5}$$

The change in LHC optics commissioning strategy implemented in 2017, to consider optics quality with the operational configuration of the crossing-scheme, therefore represents a significant gain in regard to operation of the collider. Commissioning of the LHC optics performed prior to 2017 exclusively focused on the linear optics at flat-orbit. From results presented in Sec. 3 & 4 however, it can be

Table 11: β^* obtained for the operational configuration of the IR crossing-scheme for $\beta^* = 0.4\,\mathrm{m}$ ATS optics in 2017 (before and after linear re-optimization), contrasted to the optics quality obtained for the nominal LHC optics at flat-orbit in 2016.

	2017 ATS (OP-crossing) before re-optimization			
	Beam 1 [cm]	Beam 2 [cm]		
$\beta_x^*\|_{\mathrm{IP1}}$	40.4 ± 0.1	39.0 ± 0.1		
$\beta_y^*\|_{\mathrm{IP1}}$	38.5 ± 0.1	41.3 ± 0.2		
$\beta_x^*\|_{\mathrm{IP5}}$	40.6 ± 0.1	40.5 ± 0.2		
$\beta_y^*\|_{\mathrm{IP5}}$	40.3 ± 0.1	41.6 ± 0.3		
	2017 ATS (OP-crossing) after re-optimization		**2016 Nominal (flat-orbit)**	
	Beam 1 [cm]	Beam 2 [cm]	Beam 1 [cm]	Beam 2 [cm]
$\beta_x^*\|_{\mathrm{IP1}}$	39.9 ± 0.1	39.9 ± 0.1	39.8 ± 0.5	39.8 ± 0.1
$\beta_y^*\|_{\mathrm{IP1}}$	40.8 ± 0.4	40.1 ± 0.1	40.1 ± 0.1	40.1 ± 0.1
$\beta_x^*\|_{\mathrm{IP5}}$	40.3 ± 0.2	40.2 ± 0.1	39.9 ± 0.2	39.5 ± 0.1
$\beta_y^*\|_{\mathrm{IP5}}$	40.2 ± 0.2	39.6 ± 0.1	40.1 ± 0.1	39.6 ± 0.2

surmised that nonlinear errors and the crossing-scheme represent a contribution to the beta-beat at the level of $\sim 1-2\,\%$ at $\beta^* = 0.4\,\mathrm{m}$. This contribution to the linear optics errors was neither considered nor corrected in previous years, thus earlier results relating to linear optics control at low-β^* in the LHC [7] may actually represent a slight overestimate of the optics quality achieved during actual operation of the collider for luminosity production. Through correction of the nonlinear errors and linear optics with the IR crossing-scheme applied however, it has been possible to recover the same linear optics quality in regular LHC operation as was previously obtained at flat-orbit. Compensation of the linear optics in the true operational configuration now represents a standard component of LHC commissioning strategy. Table 12, for example, shows the beta-beat obtained for the operational crossing-scheme at $\beta^* = 0.3\,\mathrm{m}$, which has also been used for operation in 2017 and 2018. With further iteration of the optics corrections in the operational configuration at $\beta^* = 0.3\,\mathrm{m}$ the RMS β-beat has further improved compared to $\beta^* = 0.4\,\mathrm{m}$ commissioning, while control of β^* remains around the $1-2\,\%$ level.

Table 12: β^* obtained for the operational configuration of the IR crossing-scheme for $\beta^* = 0.3\,\mathrm{m}$ ATS optics in 2017.

	2017 ATS (OP-crossing)	
	Beam 1	Beam 2
$\beta_x\|_{\mathrm{RMS}}$	$2.0\,\%$	$1.8\,\%$
$\beta_y\|_{\mathrm{RMS}}$	$1.8\,\%$	$1.7\,\%$
$\beta_x^*\|_{\mathrm{IP1}}$ [cm]	30.7 ± 0.2	30.0 ± 0.3
$\beta_y^*\|_{\mathrm{IP1}}$ [cm]	30.5 ± 0.2	30.0 ± 0.1
$\beta_x^*\|_{\mathrm{IP5}}$ [cm]	30.7 ± 0.2	29.8 ± 0.1
$\beta_y^*\|_{\mathrm{IP5}}$ [cm]	30.1 ± 0.1	30.4 ± 0.2
Luminosity imbalance	$0.2\,\% \pm 0.6\,\%$	

5 Conclusions

Prior to 2017, the low-β^* optics commissioning strategy for the LHC was exclusively concerned with linear optics. Since 2017 this procedure has undergone a major revision, extending the strategy to encompass also nonlinear magnetic errors in low-β^* insertions, and to account for perturbation of the linear optics by feed-down from such nonlinear errors when crossing-angle orbit bumps are applied in the experimental IRs. Commissioning strategy has in essence moved from a purely linear approach to a combined linear and nonlinear commissioning. This alternative strategy continued to be depolyed and refined during 2018 operation, and combined linear/nonlinear commissioning is forseen to become a mainstay of LHC operation for the remainder of it's life.

Where previously no nonlinear corrections were applied in the low-β^* insertions of the LHC, beam-based corrections have now been implemented for normal and skew octupole, and normal and skew sextupole errors, yielding a range of operational benefits. Normal octupole correction eliminated radical distortions of the tune footprint through the β^* squeeze, providing a stable baseline upon which to implement Landau damping of instabilities. The normal octupole correction also markedly improved the performance of beam instrumentation, specifically the continuous measurement of tune and coupling via the LHC BBQ system. This was essential in order to obtain the high-quality K-modulation data necessary to correct β^* and luminosity imbalance at end-of-squeeze. Correction of the sextupoles and skew octupoles also significantly improved the stability of tune-separation and linear coupling as a function of crossing-angle. Since Landau damping in the LHC is critically dependent on the magnitude of the linear coupling compared to the tune-separation, the nonlinear corrections played a significant role in facilitating the introduction of crossing-angle levelling into LHC operation since 2017.

Where results from linear optics commissioning have previously been reported, only the optics measured with a flat closed-orbit (an orbit with the operational crossing-angle bumps in the experimental insertions removed) was considered. A non-negligible change to the β-beat was observed however, as function of the crossing-angle. Arising from feed-down of nonlinear errors in the low-β IRs, this represents an additional source of linear optics imperfections present in the true operational configuration, which had not been considered earlier in LHC operation. To obtain the high-quality optics control desired in the LHC, it is therefore necessary to also consider the role nonlinear sources in the experimental IRs play in perturbing the linear optics.

Correction of normal sextupole errors in the CMS insertion helped improve the stability of the linear optics as a function of the crossing-scheme. After all nonlinear corrections were applied however, a non-negligible deterioration to the full operational configuration still remained (relative to the optics quality obtained during initial commissioning at flat-orbit). The linear commissioning strategy was therefore extended, to include a re-optimization of β^*; global β-beat; and normalized dispersion, with the operational crossing-scheme applied (and after application of the nonlinear corrections). This was the first time linear optics measurements at the LHC were performed with the crossing-angle orbit bumps applied. An update to the K-modulation method was required, to measure with an orbit feed-back operational, in order to minimize distortion of the tune modulation by feed-down from nonlinear magnets in the arcs and from any residual nonlinearities in the IRs. After re-optimization, a linear optics quality was achieved which is comparable to that obtained at flat-orbit in 2017 and in previous years.

Correction of nonlinear errors in low-β insertions is a question of longstanding interest to various current and historical colliders, as well as an emerging challenge for new machines such as the HL-LHC, FCC and Super-KEK. Beam-based correction of multiple species of nonlinear errors in the low-β^* IRs, and for the influence of these nonlinearities on the linear optics, has been achieved for the first time in the LHC using a variety of different linear and nonlinear observables. The corrections have been applied in regular operation with clear benefit to the machine. Of particular relevance to future colliders, such as the HL-LHC and FCC, the IR-nonlinear correction significantly improved the lifetime of the LHC beams during dedicated tests at very small $\beta^* = 0.14\,\mathrm{m}$ (well below the values currently used in LHC operation but of relevance to HL-LHC operation). Several key resonance driving terms, corresponding to the $4Q_x$

and $3Q_y$ resonances, were also reduced upon application of the relevant multipole corrections. The revised LHC commissioning strategy, based on a combined commissioning of the linear and nonlinear optics, represents a new approach which will be applied in future LHC operations and provides an initial template for commissioning of the HL-LHC in the coming years.

6 Acknowledgments

Profuse thanks go to the CERN operations group and LHC Engineers In Charge for the extensive support lent to the LHC commissioning and machine development studies which contributed to the results presented here. Similar thanks go to the LHC collimation team for helping facilitate the large amplitude beam excitations necessary for the nonlinear commissioning, and to the Beam Instrumentation group for their continual support of all the optics studies done on the LHC. Finally many thanks go to the magnet field quality (FiDeL) team at CERN for many productive discussions regarding the field quality in the LHC insertions.

References

[1] R. Tomás, O. Bruning, M. Giovannozzi, P. Hagen, M. Lamont, F. Schmidt, G. Vanbavinckhove, M. Aiba, R. Calaga, and R. Miyamoto. CERN Large Hadron Collider optics model, measurements, and corrections. *Phys. Rev. ST. Accel. Beams*, 13(121004), 2010. URL http://prst-ab.aps.org/abstract/PRSTAB/v13/i12/e121004.

[2] G. Vanbavinckhove. *Optics measurements and corrections for colliders and other storage rings*. PhD thesis, Universiteit van Amsterdam, 2012. URL https://cds.cern.ch/record/1533084?ln.

[3] A. Langner and R. Tomás. Optics measurement algorithms and error analysis for the proton energy frontier. *Phys. Rev. ST. Accel. Beams*, 18(031002), 2015. URL https://journals.aps.org/prstab/pdf/10.1103/PhysRevSTAB.18.031002.

[4] R. Tomás, T. Bach, J. Coello, V. Kain, M. Kuhn, A.S. Langner, Y.I. Levinsen, K.S.B Li, E.H. Maclean, V. Maier, N. Magnin, M.J. McAteer, T.H.B. Persson, P.K. Skowronski, R. Westenberger, and S. White. Prospects for the LHC optics measurements and corrections at higher energy. In *Proceedings of IPAC'14*, number TUPRO018, 2014. URL http://accelconf.web.cern.ch/AccelConf/IPAC2014/papers/tupro018.pdf.

[5] M. Aiba, S. Fartoukh, A. Franchi, M. Giovannozzi, V. Kain, M. Lamont, R. Tomás, G. Vanbavinckhove, J. Wenninger, F. Zimmermann, R. Calaga, and A. Morita. First β-beating measurement and optics analysis for the CERN Large Hadron Collider. *Phys. Rev. ST. Accel. Beams*, 12(081002), 2009. URL http://prst-ab.aps.org/abstract/PRSTAB/v12/i8/e081002.

[6] R. Tomás, R. Calaga, A. Langner, Y.I. Levinsen, E.H. Maclean, T.H.B. Persson, P.K. Skowronski, M. Stzelczyk, G. Vanbavinckhove, and R. Miyamoto. Record low β-beating in the LHC. *Phys. Rev. ST. Accel. Beams*, 15(091001), 2012. URL http://prst-ab.aps.org/abstract/PRSTAB/v15/i9/e091001.

[7] T. Persson, F. Carlier, J. Coello de Portugal, A. Garcia-Tabares Valdivieso, A. Langner, E.H. Maclean, L. Malina, P. Skowronski, B. Salvant, R. Tomás, and A.C. Garcia Bonilla. LHC optics commissioning: A journey towards 1% optics control. *Phys. Rev. Accel. Beams*, 20(061002), 2017. URL https://journals.aps.org/prab/abstract/10.1103/PhysRevAccelBeams.20.061002.

[8] L.C. Teng. Error analysis for the low-β quadrupoles of the Tevatron collider. Technical report, 1982. URL http://inspirehep.net/record/177853. FERMILAB-TM-1097.

[9] J. Wei and M. Harrison. The RHIC project - design, status, challenges, and perspectives. In *Multi-GeV high-performance accelerators and related technology. Proceedings, 16th RCNP International Symposium, Osaka, Japan, March 12-14, 1997*, number C97-03-12.1 p.198-206, 1997. URL www.rhichome.bnl.gov/AP/ap_notes/RHIC_AP_123.ps. FERMILAB-TM-1097.

[10] O. Brüning et al. (eds.). *LHC Design Report v.1: the LHC Main Ring*. CERN, 2004. URL https://cds.cern.ch/record/782076?ln.

[11] F. Pilat, Y. Luo, N. Malitsky, and V.Ptitsyn. Beam-based non-linear optics corrections in colliders. In *Proceedings of PAC'05*, number WOAC007, 2005. URL http://accelconf.web.cern.ch/AccelConf/p05/PAPERS/WOAC007.PDF.

[12] W. Fischer, J. Beebe-Wang, Y. Luo, S. Nemesure, and L. Rajulapati. RHIC proton beam lifetime increase with 10- and 12-pole correctors. In *Proceedings of IPAC 2010*, number THPE099, 2010. URL http://accelconf.web.cern.ch/AccelConf/IPAC10/papers/thpe099.pdf.

[13] G. Apollinari, I. Béjar Alonso, O. Bruning, M. Lamont, and L. Rossi. High-Luminosity Large Hadron Collider (HL-LHC) : Preliminary Design Report. Technical report, 2015. URL https://cds.cern.ch/record/2116337?ln. CERN-2015-005.

[14] M. Giovannozzi, S. Fartoukh, and R. De Maria. Specification of a system of correctors for the triplets and separation dipoles of the LHC upgrade. In *Proc. IPAC'13, Shanghai, China*, number WEPEA048, 2017. URL http://accelconf.web.cern.ch/AccelConf/IPAC2013/papers/wepea048.pdf.

[15] M. Giovannozzi. Field quality and DA. 6th HL-LHC Collaboration Meeting (14-16 November 2016, Paris, Espace St Martin). URL https://indico.cern.ch/event/549979/contributions/2263210/.

[16] F. Carlier, J. Coello, S. Fartoukh, E. Fol, A. García-Tabares, M. Giovannozzi, M. Hofer, A. Langer, E.H. Maclean, L. Malina, L. Medina, T.H.B. Persson, P. Skowronski, R. Tomás, F. Van der Veken, and A. Wegscheider. Optics Measurement and Correction Challenges for the HL-LHC. Technical report, 2017. URL https://cds.cern.ch/record/2290899. CERN-ACC-2017-0088.

[17] H. Sugimoto. SuperKEKB. Presentation at CERN-ICFA Workshop on Advanced Optics Control, 2015. URL https://indico.cern.ch/event/349643/overview.

[18] Daniel Schulte. Optics challenges for future hadron colliders. Presentation at CERN-ICFA Workshop on Advanced Optics Control, 2015. URL https://indico.cern.ch/event/349643/overview.

[19] M. Benedikt, D. Schulte, J. Wenninger, and F. Zimmerman. Challenges for highest energy circular colliders. Technical report, 2014. URL https://cds.cern.ch/record/1742294. CERN-ACC-2014-0153.

[20] E. Cruz-Alaniz, A. Seryi, E.H. Maclean, R. Martin, and R. Tomás. Non linear field correction effects on the dynamic aperture of the FCC-hh. In *Proc. IPAC 17. Copenhagen, Denmark*, number TUPVA038, 2017. URL http://accelconf.web.cern.ch/AccelConf/ipac2017/papers/tupva038.pdf.

[21] S. White, E. Maclean, and R. Tomás. Direct amplitude detuning measurement with ac dipole. *Phys. Rev. ST. Accel. Beams*, 16(071002), 2013. URL http://prst-ab.aps.org/abstract/PRSTAB/v16/i7/e071002.

[22] E.H. Maclean. Nonlinear optics commissioning in the LHC. Proceedings of the 7th Evian Workshop (Evian, 13-15 December 2016), 2016. URL https://indico.cern.ch/event/578001/contributions/2366314/attachments/1374391/2158727/2016_EvianPaper.pdf.

[23] L.R. Carver, M. Schenk, R. de Maria, K. Li, D. Amorim, N. Biancacci, X. Buffat, E. Maclean, E. Metral, K. Lasocha, T. Lefevre, T. Levens, and B. Salvant. MD1831: Single Bunch Instabilities with Q" and Non-Linear Errors. Technical report, 2017. URL https://cds.cern.ch/record/2253143?ln. CERN-ACC-NOTE-2017-0012.

[24] E.H. Maclean, R. Tomás, F. Schmidt, and T.H.B. Persson. Measurement of LHC nonlinear observables using kicked beams. *Phys. Rev. ST. Accel. Beams*, 17(081002), 2014. URL https://journals.aps.org/prstab/abstract/10.1103/PhysRevSTAB.17.081002.

[25] E.H. Maclean. Non-linear modelling and machine set-up. Presentation at LHC OMC review, 2013. URL http://indico.cern.ch/getFile.py/access?contribId=5&sessionId=0&resId=1&materialId=slides&confId=246159.

[26] E.H. Maclean, F. Carlier, M. Giovannozzi, T.H.B. Persson, and R. Tomás. Effect of linear coupling on nonlinear observables at the LHC. In *Proc. IPAC'17, Copenhagen, Denmark*, number WEPIK092, 2017. URL http://accelconf.web.cern.ch/AccelConf/ipac2017/papers/wepik092.pdf.

[27] E.H. Maclean T. Persson, R. Tomaás, and Y.I. Levinsen. Non-linear coupling studies in the LHC. In *Proceedings of IPAC 2015 (Richmond, VA, USA)*, number TUPTY042, 2015. URL http://accelconf.web.cern.ch/AccelConf/IPAC2015/papers/tupty042.pdf.

[28] R. Tomás, T.H.B. Persson, and E.H. Maclean. Amplitude dependent closest tune approach. *Phys. Rev. Accel. Beams*, 19(071003), 2016. URL http://journals.aps.org/prab/abstract/10.1103/PhysRevAccelBeams.19.071003.

[29] T.H.B. Persson, M. Gasior, E.H. Maclean, O. Jakub, R. Tomás, D. Valuch, D.A. Wierichs, and F.S. Carlier. Suppression of Amplitude dependent closest tune approach and first tests of the ADT as an AC-dipole (MD 1412). Technical report, 2016. URL https://cds.cern.ch/record/2220704?ln. CERN-ACC-Note-2016-0057.

[30] E.H. Maclean, T.H.B. Persson, and R. Tomás. Amplitude dependent closest tune approach generated by normal and skew octupoles. In *Proc. IPAC'17, Copenhagen, Denmark*, number WEPIK091, 2017. URL http://accelconf.web.cern.ch/AccelConf/ipac2017/papers/wepik091.pdf.

[31] L.R. Carver, D. Amorim, N. Biancacci, X. Buffat, K.S.B. Li, E. Métral, B. Salvant, and M. Schenk. Destabilising effect of linear coupling in the LHC. In *Proc. IPAC'17, Copenhagen, Denmark*, number THPAB040, 2017. URL http://accelconf.web.cern.ch/AccelConf/ipac2017/papers/thpab040.pdf.

[32] L.R. Carver, X. Buffat, K. Li, E. Metrel, and M. Schenk. Transverse beam instabilities in the presence of linear coupling in the Large Hadron Collider. *Phys. Rev. Accel. Beams*, 21(044401), 2018. URL https://journals.aps.org/prab/pdf/10.1103/PhysRevAccelBeams.21.044401.

[33] R. Calaga, R. Tomás, and F. Zimmerman. BPM calibration independent LHC optics correction. Technical report, 2007. URL http://cds.cern.ch/record/1058520?ln. CERN-LHC-PROJECT-Report-1039.

[34] R. Tomás, O. Bruning, S. Fartoukh, M. Giovannozzi, Y. Papaphilippou, F. Zimmermann, R. Calaga, S. Peggs, and A. Franchi. Procedures and accuracy estimates for beta-beat correction in the LHC. In *Proceedings of EPAC*, number WEPCH047, 2006. URL http://cds.cern.ch/record/972668?ln.

[35] R. Tomás, M. Aiba, A. Franchi, and U. Iriso. Review of linear optics measurement and correction for charged particle accelerators. *Phys. Rev. Accel. Beams*, 20(054801), 2017. URL https://journals.aps.org/prab/abstract/10.1103/PhysRevAccelBeams.20.054801.

[36] S. Fartoukh. Towards the LHC Upgrade using the LHC well-characterized technology. Technical report, 2012. URL http://cds.cern.ch/record/1301180?ln. CERN-sLHC-PROJECT-Report-0049.

[37] S. Fartoukh. Achromatic telescopic squeezing scheme and application to the LHC and its luminosity upgrade. *Phys. Rev. Accel. Beams*, 16(111002), 2013. URL https://journals.aps.org/prab/abstract/10.1103/PhysRevSTAB.16.111002.

[38] S. Fartoukh, R. Bruce, F. Carlier, J. Coello De Portugal, A. Garcia-Tabares, E. Maclean, L. Malina, A. Mereghetti, D. Mirarchi, T. Persson, M. Pojer, L. Ponce, S. Redaelli, B. Salvachua, P. Skowronski, M. Solfaroli, R. Tomás, D. Valuch, A. Wegscheider, and J. Wenninger. Experimental validation of the Achromatic Telescopic Squeezing (ATS) scheme at the LHC. *IOP Conf. Series: Journal of Physics*, 874(012010), 2017. URL http://iopscience.iop.org/article/10.1088/1742-6596/874/1/012010/pdf.

[39] A. Franchi. *Studies and Measurements of Linear Coupling and Nonlinearities in Hadron Circular Accelerators*. PhD thesis, Universität Frankfurt, 2006. URL http://www.gsi.de/en/start/beschleuniger/fachabteilungen/accelerator_physics/phd_thesis.htm.

[40] R. Calaga, R. Tomás, and A. Franchi. Betatron coupling: Merging Hamiltonian and matrix approaches. *Phys. Rev. ST. Accel. Beams*, 8(034001), 2005.

[41] T. Persson and R. Tomás. Improved control of the betatron coupling in the Large Hadron Collider. *Phys. Rev. ST. Accel. Beams*, 17(051004), 2014.

[42] E.H. Maclean, F.S. Carlier, S. Fartoukh, T.H.B. Persson, P.K. Skowronski, R. Tomás, and D.A. Wierichs. Demonstration of coupling correction below the per-mil limit in the LHC. Technical report, 2016. URL https://cds.cern.ch/record/2210530?ln. CERN-ACC-NOTE-2016-0053.

[43] T. Persson, G. Baud, X. Buffat, J. Coello de Portugal, E. Fol, K. Fuchsberger, M. Gabriel, M. Giovannozzi, G.H. Hemelsoet, M. Hostettler, M. Hruska, D. Jacquet, E.H. Maclean, L. Malina, J. Olexa, P. Skowronski, M. Soderen, M. Solfaroli Camillocci, R. Tomaś, D. Valuch, A. Wegscheider, and J. Wenninger. Transverse coupling measurements with high intensity beams using driven oscillations. In *Proceedings of IPAC 2018, Vancouver, BC, Canada*, number MOPMF047, 2018. URL http://ipac2018.vrws.de/papers/mopmf047.pdf.

[44] T.H.B. Persson, Y.I. Levinsen, R. Tomás, and E.H. Maclean. Chromatic Coupling Correction in the Large Hadron Collider. *Phys. Rev. ST. Accel. Beams*, 16(081003), 2013. URL http://prst-ab.aps.org/abstract/PRSTAB/v16/i8/e081003.

[45] CERN FiDeL group documentation on the magnetic model of the LHC. Technical report. URL https://lhc-div-mms.web.cern.ch/lhc-div-mms/tests/MAG/Fidel/.

[46] O. Bruning, S. Fartoukh, M. Giovannozzi, and T. Risselada. Dynamic Aperture Studies for the LHC Separation Dipoles. Technical report, 2004. URL https://cds.cern.ch/record/742967?ln. LHC Project Note 349.

[47] R. Tomás, M. Giovannozzi, and R. de Maria. Nonlinear correction schemes for the phase 1 LHC insertion region upgrade and dynamic aperture studies. *Phys. Rev. Spec. Top. Accel. Beams*, 12 (011002), 2009. URL https://cds.cern.ch/record/1159657.

[48] E.H. Maclean, R. Tomás, M. Giovannozzi, and T.H.B. Persson. First measurement and correction of nonlinear errors in the experimental insertions of the CERN Large Hadron Collider. *Phys. Rev. Spec. Top. Accel. Beams*, 18(121002), 2015. URL http://journals.aps.org/prab/abstract/10.1103/PhysRevSTAB.18.121002.

[49] S. Mönig, E.H. Maclean, T.H.B. Persson, J.M. Coello de Portugal, A. Langner, and R. Tomás. Short Term Dynamic Aperture with AC Dipoles. In *Proceedings of IPAC 16*, number THPMR044, 2016. URL http://accelconf.web.cern.ch/AccelConf/ipac2016/papers/thpmr044.pdf.

[50] F.S. Carlier, R. Tomás, E.H. Maclean, and T.H.B. Persoon. First Demonstration of Dynamic Aperture Measurements with an AC dipole. In preparation.

[51] E.H. Maclean, F.S. Carlier, J.M. Coello de Portugal, A. Garcia-Tabares, M. Giovannozzi, L. Malina, T.H.B Persson, P.K. Skowronski, and R. Tomás. New methods for measurement of nonlinear errors in LHC experimental IRs and their application in the HL-LHC. In *Proc. IPAC'17. Copenhagen, Denmark*, number WEPIK093, 2017. URL http://accelconf.web.cern.ch/AccelConf/ipac2017/papers/wepik093.pdf.

[52] F. Carlier, R. Tomás, and E.H. Maclean. In preparation, 2018.

[53] A. Boccardi, M. Gasior, R. Jones, and R.J. Steinhagen. An overview of the LHC Transverse Diagnostics Systems. Technical report, 2009. URL http://cds.cern.ch/record/1156346?ln. LHC Project Report 1166.

[54] M. Gasior and R. Jones. The principle and first results of betatron tune measurement by direct diode detection. Technical report, 2005. URL http://cds.cern.ch/record/883298?ln. LHC-Project-Report 853.

[55] R. Tomás. Normal form of particle motion under the influence of an ac dipole. *Phys. Rev. ST. Accel. Beams*, 5(054001), 2002. URL https://journals.aps.org/prab/abstract/10.1103/PhysRevSTAB.5.054001.

[56] F. Carlier, R. Tomás, E.H. Maclean, and T.H.B. Persson. Nonlinear correction strategies for the LHC using Resonance Driving Terms. In *Proceedings of IPAC 18*, number MOPFM032, 2018.

[57] MAD - Methodical Accelerator Design. URL http://mad.web.cern.ch/mad/.

[58] É. Forest, F. Schmidt, and E. McIntosh. Introduction to the Polymorphic Tracking Code. Technical report, 2002. URL http://cds.cern.ch/record/573082/files/sl-2002-044.pdf. CERN-SL-2002-044 (AP).

[59] E.H. Maclean, J.W. Dilly, F.S.. Carlier, M. Hofer, and R. Tomás. Report from LHC MD 3311: Amplitude detuning at end-of-squeeze. Technical report, 2018. In preparation.

[60] E.H. Maclean, M. Giovannozzi, T.H.B. Persson, R. Tomás, and J. Wenninger. Understanding the tune, coupling, and chromaticity dependence of the LHC on Landau octupole powering. Technical report, 2013. URL https://cds.cern.ch/record/1541981?ln. CERN-ATS-Note-2013-023 TECH.

[61] E.H. Maclean, M. Giovannozzi, W. Herr, Y.I. Levinsen, G. Papotti, T.H.B. Persson, P.K. Skowronski, R. Tomás, and J. Wenninger. Understanding the tune, coupling, and chromaticity dependence of the LHC on Landau octupole powering. In *Proc. IPAC'13, Shanghai, China*, number TUPWO048, 2013. URL http://accelconf.web.cern.ch/AccelConf/IPAC2013/papers/tupwo048.pdf.

[62] D.A. Wierichs, F. Carlier, E.H. Maclean, T.H.B. Persson, J.M.C. Portugal, and R. Tomás. C^- error bars and the influence of noise on the coupling measurement. Technical report, 2016. Unpublished.

[63] F.S.. Carlier, J.M. Coello de Portugal, J.W. Dilly E. Fol, A. Garcia-Tabares Valdivieso, E.H. Maclean, L. Malina, T.H.B. Persson, P.K. Skowronski, and R. Tomás. MD2723 - Amplitude Detuning Studies at 6.5 TeV with Various Configurations of the Crossing Scheme. Technical report, 2018. URL http://cds.cern.ch/record/2306325. CERN-ACC-NOTE-2018-0022.

[64] S. Fartoukh et. al. ATS MD's in 2016. Technical report, 2017. URL https://cds.cern.ch/record/2242513?ln. CERN-ACC-2017-0003.

[65] E.H. Maclean, F. Carlier, M.S Camillocci, K. Fuchsberger, M. Giovannozzi, T.H.B. Persson, and R. Tomás. Report from LHC MDs 1391 and 1483: Tests of new methods for study of nonlinear errors in the LHC experimental insertions. Technical report, 2017. URL http://cds.cern.ch/record/2314410. CERN-ACC-NOTE-2018-0035.

[66] E.H. Maclean, R. Tomás, T.H.B. Persson, and F.S. Carlier. Report from LHC MD 2171: Amplitude dependent closest tune approach from normal and skew octupoles. Technical report, 2018. URL http://cds.cern.ch/record/2310163. CERN-ACC-Note-2018-0027.

[67] G. Guignard. Betatron coupling and related impact of radiation. *Phys. Rev. E*, 51(6), 1995. URL https://cds.cern.ch/record/300856?ln.